UM HE 70-4

THE UNIVERSITY OF MICHIGAN
COLLEGE OF LITERATURE, SCIENCE, AND THE ARTS
Department of Physics

Technical Report

MULTIPARTICLE PRODUCTION IN LIQUID HYDROGEN AND CARBON BY CHARGED COSMIC RAY HADRONS OF ENERGY GREATER THAN 70 GeV

K. N. Erickson

ORA Project 03028

supported by:

NATIONAL SCIENCE FOUNDATION
GRANT NO. GP-13265
Washington, D.C.

administered through:

OFFICE OF RESEARCH ADMINISTRATION ANN ARBOR

April 1970

The research reported in this thesis is a part of the Michigan-Wisconsin cosmic ray program at Echo Lake, Colorado. K. N. Erickson and his thesis professor, P. D. Kearney, have been associated with this experiment since its inception. This program has been supported by the National Science Foundation grants GP8332 and GP13265.

ABSTRACT

HIGH ENERGY MULTIPARTICLE PRODUCTION IN LIQUID HYDROGEN AND CARBON BY CHARGED COSMIC RAY HADRONS OF ENERGY GREATER THAN 70 GeV

The operation of a cosmic ray experiment at Echo Lake, Colorado from March, 1968 to May, 1969 produced 288 and 681 in-geometry interactions respectively from a carbon and a liquid hydrogen target. The energy of these interactions was greater than 70 GeV as measured by an ionization calorimeter. A study has been made as to the energy dependence of average charged multiplicity and inelasticity, as well as the multiplicity distributions and the center of mass angular distributions of the charged particles in the final state. It was found that the average charged multiplicity increases with energy in very good agreement with the ln E dependence as predicted by the multiperipheral model of Chew and Pignotti. The multiplicity distributions were found to be Poisson in nature, consistent with the predictions of Chew and Pignotti and C. P. Wang. The inelasticity was found to be independent of the primary energy. The center of mass angular distributions were observed to be non-isotropic. Results in

hydrogen and carbon have been compared with respect to average charged multiplicity and inelasticity.

Kenneth Neil Erickson
Physics Department
Colorado State University
Fort Collins, Colorado
June, 1970

ACKNOWLEDGMENTS

I would like to take this opportunity to express my appreciation to all the people who have worked on the Echo Lake experiment. In particular, the helpful assistance of Dr. L. W. Jones, Dr. D. E. Lyon, Dr. A. E. Bussian, G. DeMeester, B. Loo, Dr. R. Roth and Dr. P. V. Ramana Murthy of the University of Michigan and Dr. F. E. Mills, Dr. D. D. Reeder, Dr. J. Learned and J. Wilkes of the University of Wisconsin and Dr. B. Cork of Argonne National Laboratory, is gratefully acknowledged.

It is also my pleasure to thank Dr. P. D. Kearney, who introduced me to the Echo Lake experiment and served as my dissertation advisor at Colorado State University.

The hospitality of the physics departments at the University of Wisconsin and the University of Michigan, where the data analysis for this work was accomplished, is also gratefully acknowledged. In addition, I would like to thank the University of Denver for the use of their Echo Lake laboratory facilities and the National Center for Atmospheric Research at Boulder, Colorado for the use of their computing facility during the earlier stages of the analysis. The engineering and technical assistance of the Physical Sciences Laboratory of the University of Wisconsin, in particular the

work of W. Winter, J. Hicks and R. Brown was greatly appreciated.

This work was supported by the National Science Foundation. In addition, the National Aeronautics and Space Administration is acknowledged for their support, during three years of my graduate work under their NASA traineeship program.

Lastly, I would like to thank my wife, Sharon, for her encouragement and help throughout the course of this work.

TABLE OF CONTENTS

LIST OF TABLES

LIST OF FIGURES

LIST OF FIGURES (Continued)

CHAPTER I

BACKGROUND

The Echo Lake, Colorado cosmic ray facility was designed to investigate some of the features of nucleon-nucleon and nucleon-nucleus collisions in the energy range 50-1000 GeV. Reported in this paper are the results obtained from a study of the inelastic interactions produced by charged cosmic ray hadrons in two target materials: liquid hydrogen and carbon. Specifically studied were the multiplicity distributions of charged particles in the final state, average charged multiplicities and center-of-mass angular distributions.

Presented in this initial chapter are some introductory remarks regarding the general features of high energy multiparticle production and the motivations of the Echo Lake experiment. This is followed by a discussion of the various model predictions and approaches of study directly related to the specific features of multiparticle production reported in this paper.

A. Introduction

At energies greater than those currently achieved in accelerator experiments, approximately 30 GeV, the present knowledge concerning multiparticle production is based on the analysis of collisions of cosmic ray hadrons with a variety of

target materials. These investigations, together with those at accelerator energies, have revealed certain general features of the phenomenon and a number of models have been proposed to account for the observed facts. At present there is no single model which is capable of explaining all of the observed behavior. As most of the present models have been formulated in terms of nucleon-nucleon collisions it is important, for purposes of comparison, to provide experimental information about such collisions at cosmic ray energies. All previous cosmic ray experiments designed to study the properties of strong interactions have employed targets heavier than hydrogen. In targets of complex nuclei the interaction occurs within a nucleus and it is difficult to assure that only one nucleon is involved in the collision. Various criterion have been applied in these experiments in order to select as pure a sample of nucleon-nucleon collisions as possible. The general features of nucleon-nucleon collisions as deduced by such experiments have been summarized by G. Jarlskog[1] A somewhat more complete summary, including results from both accelerator and cosmic ray experiments, has been given by S. Yamada and M. Koshiba[2]. These authors have also included an extensive list of the experimental references and a list of the various models proposed prior to 1967. In addition Barashenkov, et al.[3], have made an extensive survey of the experimental data

involving the inelastic interactions of hadrons. Both cosmic ray and accelerator data up through 1965 has been included.

For purposes of completeness and future reference, the general features of high energy nucleon-nucleon collisions which are of the most direct interest to this paper, as abstracted from the above references, have been summarized below.

1. The average multiplicity of the final state particles is a slowly increasing function of the primary energy. Previous cosmic ray measurements, within the experimental errors, are consistent with either a ℓnE or $E^{\frac{1}{4}}$ dependence on primary energy. Measurements of average multiplicities as a function of energy are important in that most model predictions are very specific about the energy dependence of this quantity.

2. The inelasticity, defined in the lab. system as the fraction of the incident energy carried away by created particles, has been found on the average to equal approximately 0.5, independent of primary energy.

3. Over a range of primary energy from several tens of GeV to tens of thousands of GeV, approximately 70-80% of the produced particles are pions. At accelerator energies the proportion of kaons is about 10%.

4. The angular distributions of the secondary particles show in many cases a forward-backward peaking in the center-of-mass (C.M.) system.

5. The mean transverse momentum of the produced particles is constant at a C. M. value of approximately 0.4 GeV/c and depends on neither the primary energy (up to at least 10^4 GeV) nor the emission angle, except possibly in the extreme forward and/or backward directions.

There were three primary motivations for the Echo Lake cosmic ray facility. First, a liquid hydrogen target was employed in order to eliminate the ambiguities involved in selecting nucleon-nucleon collisions from interactions in heavier targets. Secondly, one of the principle problems in cosmic ray experiments has been the determination of the primary energy of the incident particle. Various approaches have been used, such as, Coulomb scattering measurements as in the work of Lohrmann, Teucher and Schein[4], or methods where the primary energy is derived from the emission angles in the laboratory system (L. S.) of the final state particles as by the Castagnoli method[5] or that of Duller and Walker[6]. Recent Russian experiments by N. A. Dobrotin, et al.[7] and Yu. A. Eremenko, et al.[8] have employed ionization calorimeters for the determination of primary energy. In the Echo Lake experiment a large ionization calorimeter was installed and calibrated in terms of cosmic ray muons in order to determine the primary energy. The calorimeter, in addition to affording the best energy determination presently available, was not as subject to the large

event by event fluctuations observed in other methods and consequently provided a more reliable means for binning events as to energy. Thirdly, because of the steeply falling energy spectrum of primary cosmic ray nucleons ($N(E)\,dE \sim E^{-2.67}dE$)[15] the flux of cosmic ray particles falls off quite rapidly with energy and the statistics needed for reliable determination of quantities which are dependent on the total energy has in most cosmic ray experiments been inadequate. With this in mind, the Echo Lake facility was designed with a large solid angle area product of acceptance (approximately $0.7 m^2$-str.) and data was collected for a period of about seven months using the liquid hydrogen target.

The Echo Lake facility is at an altitude of 10,600 feet corresponding to an atmospheric depth of 700 gm-cm^{-2}. At these mountain altitudes there is a contamination to a pure proton flux from nuclear interactions higher in the atmosphere. The high energy nuclear active particles in the cosmic radiation at mountain altitudes consist of protons, neutrons, charged pions and, to a negligible extent, kaons. In order to unambigiously investigate proton-proton interactions it is necessary to identify the incident particle. In this experiment the neutrons posed no problem because of the triggering criterion for charged particles. However, the charged pions could not be selected out of the incoming flux. The majority of incoming charged particles at Echo Lake are,however,

protons, with the ratio of protons to protons plus pions estimated to be .67± .10 at the altitude of Echo Lake.[9] Based on this ratio about 30% of the interactions observed in this experiment were due to charged pions.

B. Multiplicity Distributions of Charged Secondaries

The observed multiplicity distributions of charged particles in the final state have been compared to two models. These models, which predict variations of a Poisson distribution for the multiplicity, are discussed briefly below.

The multiperipheral bootstrap model of Chew and Pignotti[10] applies the multi-Regge hypothesis to multiple production processes. It is assumed that the dominant mechanism is meson exchange, with baryon exchange being neglected. A simplified version further assumes that only nucleons and pions are emitted from the collision. A two parameter formula for the cross section leading to the production of n particles is given as

$$\sigma_n^{ab} = \sigma_{tot\ inel}^{ab} \frac{(g_m^2 X_o)^n}{n!} e^{-g_m^2 X_o} , \qquad (I.1)$$

where a and b refer to the 2 particles in the initial state. This formula describes the multiplicity and energy variation for all possible incident-particle combinations. For a given initial state it contains two parameters: the coupling between a and b, g_m^2,

and the constant value of the total inelastic cross section $\sigma_{\text{tot inel}}^{ab}$. The quantity X_o depends on the total energy of the system. The cross section σ_n^{ab} has the form of a Poisson distribution where the average number of produced pions (charged and neutral) is given by the product of g_m^2 and X_o.

From an experimental standpoint it is easier to present the data in terms of events characterized by a given number of charged particles (prongs) in the final state. Chew and Pignotti have determined the cross section in terms of charged prongs for the case of proton-proton collisions, based on the following assumptions. First, it is assumed that only pions are produced and secondly, that the effective meson Regge pole has the following properties: 1) it carries either isospin zero or one, 2) it occurs with equal probabilities at the ends of the multi-Regge chain with isospin zero and one, and 3) it occurs with alternating values of the isospin along the multi-Regge line. It is further pointed out by the authors that as a consequence of the above, on the average, two thirds of the pions produced will be charged. The inelastic cross section for processes with $2(i + 1)$ prongs was found to be

$$\sigma_{2(i+1)\text{prongs}}^{pp} = \sum_{n=n_{min}(i)}^{\infty} \frac{1}{2} \{ C\left[\text{Int}\left(\frac{1}{2}n\right), i\right] + C\left[\text{Int}\left(\frac{n-1}{2}\right), i\right] \} \sigma_n^{pp} , \qquad \text{(I. 2)}$$

where

$$n_{min}^{(i)} = \max(2i,\ 1)$$

Int(X) = integer part of X

$$C(m, i) = \left(\frac{2}{3}\right)^{i} \left(\frac{1}{3}\right)^{m-i} \frac{m!}{i!(m - i)!} \qquad \text{if } m \geq i$$

$$= 0 \qquad \text{if } m < i$$

and σ_n^{pp} is given by equation (I. 1). A fit of the expression (I. 2) to experimental data from proton-proton collisions in the energy range 12-29 Gev by the authors, yielded for the parameters

$$\sigma_{tot\ inel}^{pp} = 29.7 \text{ mb}$$

and

$$g_m^2 = 1.30 \quad .$$

It should be noted that a misprint occurs in the authors' paper. The value of 1. 14 given is for g_m not g_m^2. J. W. Elbert, et al.[11] have found that the form of expression (I. 2) is the same for $\pi^- p$ collisions and have found good agreement in fitting to the multiplicity distributions of charged tracks observed in 25 GeV/c $\pi^- p$ interactions. These authors obtained a value of $g_m^2 = 1.14$ from the fit, a value somewhat smaller than that found by Chew and Pignotti in fitting the pp data.

In fitting the experimental multiplicity distributions from this experiment, the fit was made in terms of numbers of events

rather than cross sections. Explicitly the form of (I. 2) used was

$$N_{2(i+1)\text{ prongs}}^{pp} = K \sum_{n=n_{min}^{(i)}}^{\infty} \frac{1}{2}\{C[\text{Int}(\tfrac{1}{2}n), i] + C[\text{Int}(\tfrac{n-1}{2}), i]\}\frac{(g_m^2 X_o)^n}{n!} e^{-g_m^2 X_o}, \qquad \text{(I. 3)}$$

where K is a normalization factor. The fit was made to the parameters, K, and the average number of produced pions

$$\langle n_\pi \rangle = g_m^2 X_o \quad .$$

C. P. Wang[12] has noted a regularity of multiplicity distributions for charged secondaries emitted from hadron collisions at accelerator energies. He has shown that the data points could be fitted by a universal set of "multiplicity distribution functions" constructed from Poisson terms. The conservation laws of charge and baryon number are incorporated into these functions. It is assumed that only pions are produced and that the production of neutral and charged pions is independent. In terms of the conservation of charge, two possibilities, denoted as Model I and Model II, are considered.

Model I.

It is assumed that charge conservation exists in a local sense inside the collision system and that charged pions are only produced in pairs from small regions or "cells". Conservation of charge at each "cell" together with the assumption that these "cells" of production are nearly independent suggests that the multiplicity distribution is Poisson in the mean number of charged pion pairs produced. The probability function for the emission of n_s charged secondaries is given as

$$W^{I}_{n_s} = \frac{\left[\left\langle \frac{n_s - \alpha}{2} \right\rangle\right]^{(n_s - \alpha)/2}}{[(n_s - \alpha)/2]!} e^{-\left\langle \frac{n_s - \alpha}{2} \right\rangle} \qquad (I.4)$$

where α is the number of charged particles in the initial state, for example $\alpha = 2$ for pp or $\pi^{\pm}$p collisions, $\alpha = 1$ for pn or $\pi^{\pm}$n collisions, and $\alpha = 0$ for nn collisions. It should be noted also that conservation of charge restricts n_s to be even or odd depending upon the initial state.

Model II.

The conservation of charge is relaxed to hold only for the whole collision system. In this case the probability function for the emission of n_s charged secondaries is given as

$$W^{II}_{n_s} = \frac{\dfrac{\langle n_s - \alpha \rangle^{(n_s - \alpha)}}{(n_s - \alpha)!} \cdot e^{-\langle n_s - \alpha \rangle}}{\sum_{\substack{n_s = \beta \\ \infty}} \dfrac{\langle n_s - \alpha \rangle^{(n_s - \alpha)}}{(n_s - \alpha)!} \cdot e^{-\langle n_s - \alpha \rangle}} \qquad \text{(I.5)}$$

where α has the same role as above and $\beta = 1(2)$ for n_s = odd (even).

In fitting the experimental data to these functions of C. P. Wang, the fit was made in terms of numbers of events. A two parameter fit was made to the average number of charged secondaries and a normalization parameter, K.

C. Average Multiplicity

There are several models which predict the energy dependence of average multiplicity in high energy nucleon-nucleon interactions. The hydrogen data on average charged multiplicities from this experiment has been compared to three of these models. The predictions of these models as to the energy dependence on average multiplicity are discussed below. Average charged multiplicity as used here is defined to be the average number of charged particles in the final state.

In the hydrodynamical model, Belenjki and Landau[13] have elaborated on the ideas advanced by Fermi[14] in the so-called statistical model of high energy meson production. As in Fermi's model, the average number of created particles is predicted to

depend on the laboratory primary energy as $E^{\frac{1}{4}}$. The hydrodynamical model speaks of the total number of particles created in the collision, as well as the initial particles. In order to fit to the observed average charged multiplicity, it was assumed that on the average two-thirds of the created particles (mainly pions) were charged and that the number of charged particles observed in the final state was equal to the number of created charged particles plus two. The functional form explicitly compared to the data was

$$\langle n_c \rangle = \frac{2}{3}(AE^{\frac{1}{4}} + 1)$$

where $\langle n_c \rangle$ was the average number of final state charged particles observed.

The multiperipheral model of Chew and Pignotti[10], as discussed previously, predicts the average number of pions produced in hadron-hadron collisions. The explicit prediction is given as

$$\langle n_\pi \rangle = g_m^2 X_o \quad .$$

For the case of pp collisions, with the target proton at rest in the L. S., the expression for X_o is just

$$X_o = \ell n \frac{E}{m}$$

where E is the laboratory primary energy of the incoming proton

and m is its rest mass. Making the same assumptions as above regarding created and observed particles, the average number of predicted pions created was related to the average number of charged particles observed by

$$\langle n_c \rangle = \frac{2}{3}(g_m^2 \ln \frac{E}{m}) + 2 \quad .$$

The isobar-pionization model proposed by Y. Pal and B. Peters[15] pictures a nucleon-nucleon collision as a two-fold process. As the two nucleons collide in the C. M. frame, a "fireball" is created at rest in that system and the incident baryons emerge as isobars with a probability, s. The evaporation of the "fireball", referred to as the pionization process, gives rise to a number of mesons whose average number increases in proportion to the energy available. The isobars in turn decay by emitting on the average n_B pions. The model requires a relation of the form

$$n_t = 2 s n_B + n_o E^{\frac{1}{2}}$$

for the total number of created particles, where the term $n_o E^{\frac{1}{2}}$ represents the created mesons in the pionization process. The energy, E, referred to here is the laboratory primary energy. As for the multiperipheral model, the average number of charged particles observed was related to the predicted number of created particles (mainly pions) by

$$\langle n_c \rangle = \frac{2}{3}(A + BE^{\frac{1}{2}}) + 2 \quad . \tag{I.8}$$

D. Angular Distributions of Secondaries

In studying the angular distributions of the charged secondaries, the approach first introduced by Duller and Walker[6] was used. This approach used previously by several authors[16 - 18] is based on a relativistic kinematical transformation between the C. M. system and the L. S. By means of this approach the energy of an event can be predicted from the angular distribution of the secondaries.

If an isotropic distribution is assumed for the secondaries in the C.M.S., where θ_i^c represents the angle of the i^{th} secondary, then the fraction of secondaries within $\theta_{c,m.}$ is given by

$$F(\theta_{c,m.}) = \frac{\int_0^{\theta_{c.m.}} \int_0^{2\pi} \frac{N_T}{4\pi} \sin\theta^c d\theta^c d\phi^c}{N_T} = \sin^2 \theta \frac{c.m.}{2} \tag{I.9}$$

where N_T is the total number of secondaries. Experimentally the fractions are determined in the L. S. so that one desires a similar expression for that system. The angle of the i^{th} secondary kinematically transforms according to

$$\tan\theta_i^L = \frac{1}{\gamma} \frac{\sin\theta_i^c}{(\frac{\beta}{\beta_i} + \cos\theta_i^c)} \tag{I.10}$$

where $\gamma = 1/\sqrt{1 - \beta^2}$ is the Lorentz factor of the C. M. and β_i is the velocity of the i^{th} secondary in the C. M. S. Assuming

$\beta/\beta_i = 1$, a good assumption for the high energy collisions, the above transformation equation reduces to

$$\tan \theta_L = \frac{1}{\gamma} \tan \frac{\theta_{c.m.}}{2} \quad . \tag{I. 11}$$

For an isotropic distribution, the fraction within $\theta_{c.m.}$ in the C. M. S. is equal to the fraction within the corresponding angle θ_L in the L. S., and by means of (I. 9) and (I. 11) it follows that

$$\frac{F(\theta_L)}{1 - F(\theta_L)} = \gamma^2 \tan^2 \theta_L \tag{I. 12}$$

or

$$\log \left(\frac{F(\theta_L)}{1 - F(\theta_L)} \right) = 2 \log \tan \theta_L + 2 \log \gamma \quad .$$

Hence, in a plot of $\log \frac{F(\theta_L)}{1 - F(\theta_L)}$ vs $\log \tan \theta_L$, if the distribution of secondaries is isotropic in the C. M. S. one expects a straight line of slope 2 and intercept $2 \log \gamma$. The Lorentz factor, γ, is most easily determined from the $F(\theta_L) = \frac{1}{2}$ point. At this point $\log \gamma = -\log \tan \theta(\frac{1}{2})$. The corresponding laboratory energy is then determined in the usual way from

$$E = (2\gamma^2 - 1)\, mc^2$$

Cocconi [19], in analyzing cosmic ray interactions, observed bimodel angular distributions of secondaries corresponding to C. M. differential number density distributions of the form

$\cos^{M}\theta_{c.m.}\, d\Omega_{c.m.}$, where M is an even integer. Duller-Walker plots, instead of showing a straight line of slope 2 corresponding to an isotropic C. M. distribution, showed two branches, each a straight line having a slope of approximately 2, symmetric with respect to the $F(\theta_L) = \frac{1}{2}$ point. This corresponded, in the L. S., to an inner and an outer cone of secondaries, or to preferential forward and backward emission in the C. M. S. Cocconi proposed a more physical picture for the observed behavior. He suggested the emission of secondaries as taking place from two centers or "fireballs" moving apart in the C. M. S. It should be pointed out that the question of whether or not "fireballs" are real or just kinematical devices, is still unanswered. Cocconi has pointed out that the idea of producing "fireballs" is not essential for describing the observed anisotropic distributions.

If a Duller-Walker analysis is carried out in terms of the inner cone (forward branch) and the outer cone (backward branch) separately, several interesting quantities can be experimentally determined.[19] In his paper Cocconi has summarized the kinematical relations, given here for future reference.

$$\gamma = (\gamma_{b_1} \gamma_{b_2})^{\frac{1}{2}} \tag{I. 13}$$

$$\gamma_F = 0.5 \left(\gamma_{b_1} / \gamma_{b_2}\right)^{\frac{1}{2}} \tag{I. 14}$$

$$\rho = \frac{(n_1 + n_2)\,\gamma_F}{2\gamma} = \frac{3}{8}\,\frac{N}{\gamma_{b_2}} \qquad \text{(I. 15)}$$

$$\gamma_N = \gamma(1 - \rho) \qquad \text{(I. 16)}$$

The quantity γ_F is the Lorentz factors of the "fireballs" with respect to the C. M. S., γ_{b_1}, γ_{b_2} are the Lorentz factors of the forward and backward moving fireballs with respect to the L. S., n_1, n_2 are the number of secondaries emitted from the forward and backward moving fireballs, $N = \frac{2}{3}(n_1 + n_2)$ is the number of charged pions emitted, assuming that the majority of secondaries are pions and two-thirds of them are charged, and γ, γ_N are the Lorentz factors of the C. M., and of the two initial nucleons with respect to the L. S. The inelasticity, ρ, is calculated from the ratio of the total energy in the two "fireballs" to the total energy in the C. M. S.

For the analysis of angular distributions of secondaries in this experiment, it was necessary to reformulate the Duller-Walker approach in a projected L. S. This was required because the events were photographed in 90° stereo and specific correlation of secondaries from the two views was not possible. Fortunately, a reformulation was possible not only for an isotropic C. M. differential number distribution, $Kd\Omega_{c.m.}$, but also for a distribution of the form $(A + B\cos^M\theta)d\Omega_{c.m.}$ where $A + B = 1$ and M is an even integer. For the isotropic case it was found that the

counterpart of equation (I. 12) has the form

$$\frac{F^2(\theta_p)}{1 - F^2(\theta_p)} = \gamma^2 \tan^2 \theta_p \quad , \tag{I. 17}$$

where θ_p refers to the angle in the projected L. S. The results for a C. M. distribution of the form $A + B \cos^M \theta$ are somewhat more involved. The reformulation has been carried out for values of M equal to 2 and 4. The results were put in the form

$$\frac{F^2(\theta_p)}{1 - F^2(\theta_p)} = (\gamma^2 \tan^2 \theta_p)\, f_M(A, B, \gamma \tan \theta_p) \quad . \tag{I. 18}$$

The details and complete results are given in Appendix A.

In analyzing the experimental distributions, two approaches were taken involving the projected Duller-Walker formulation. Plots of the data showed that the distributions were not isotropic, but rather two branches were observed, indicating a distribution of the second form. The first approach involved fitting the experimental plots to the theoretically evaluated functions. For a particular value of M, the fit was made in terms of the two parameters B and γ. B then gave a measure of the degree of deviation of the distributions from isotropic, and γ provided a measure of energy, independent of the calorimeter. In the second approach the two branches of the plots were independently fitted, in the same manner used by Cocconi, to determine γ, γ_F, γ_N and the

inelasticity, ρ. The results of these fits are presented in Chapter IV and thus will not be discussed further here.

CHAPTER II

EXPERIMENTAL PROCEDURE

Presented in this chapter is a discussion of the overall experimental arrangement, the data collection procedures, and the major components of the experiment. Because of its uniqueness in cosmic ray experiments, special attention is given to the liquid hydrogen target. The calorimeter, with regard to calibration and energy determination is also discussed in detail.

A. General Description

The overall experimental arrangement, given in Fig. 1, consisted basically of two wide-gap spark chambers of 80 x 80 in.^{2} spanning a 2000 liter liquid hydrogen target. This combination surmounted a calorimeter consisting of 10 layers of plastic scintillator and 1130 gm/cm^2 of iron. The upper 200gm/cm^2 of the calorimeter was actually a narrow-gap iron plate spark chamber. A 72 x 72 in.^{2} layer of scintillator located directly above the upper wide-gap chamber and denoted as the top counter served as part of the coincidence for acceptance of charged particles. In addition, a layer of shower counters was uniformly distributed around the stack at the level of the target center to provide a veto when accompanying particles were present. The

FIGURE 1. Experimental arrangement of the Echo Lake, Colorado cosmic ray physics facility.

EXPERIMENTAL ARRANGEMENT

FRONT VIEW

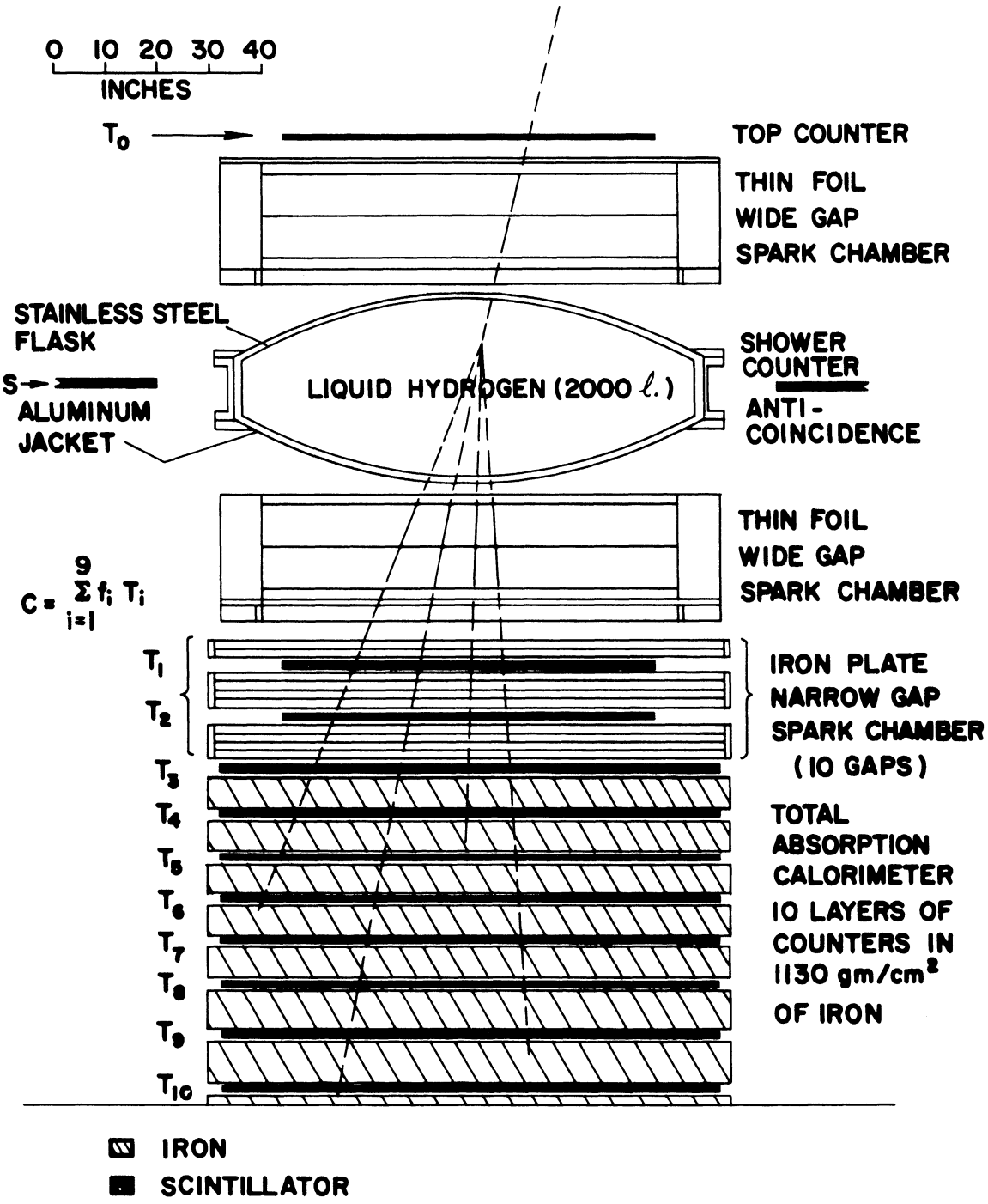

shower counters were arranged around the stack forming a square with outside dimensions of 14 x 14 ft. The overall height of the stack was 15.8 ft. and the useful geometry for acceptance of events corresponded to a solid angle-area product of 0.7 m^2 - str.

The normal criterion for the acceptance of charged hadrons consisted of a 3-fold coincidence between the top counter, the calorimeter, and the shower counters as an anti-coincidence. Normally the threshold energy for acceptance was 84 GeV, although runs were also made with a threshold of 34 GeV.

For a given event the summed output from 8 phototubes, for each of the 10 layers of the calorimeter, was recorded on magnetic tape via a logarithmic analogue-to-digital converter (LADC), a buffer, and a recorder. Also recorded on the magnetic tape was the event number, a run number and other assorted coded information. Recorded on film were the wide-gap and narrow-gap spark chambers photographed in 90 degree stero. In addition, by means of neon data lights, the appropriate coded information was also on film for each event.

B. Spark Chambers and Optics

The two wide-gap chambers had an effective cross-sectional area of 80 x 80 $in.^2$ and contained four gaps each. The three electrodes which defined the gaps were 0.002 in. aluminum foil while the walls were 32/64 in. plate glass. The two inner

(effective) gaps had 8 in. spacing and the outer two (dummy) gaps had 2 in. spacing. The dummy gaps served to equalize the pressure on each side of the outer foils. The narrow gap chamber had an effective cross-sectional area of 100 x 80 in.^{2}, contained 10 gaps and was built from copper coated iron plates $\frac{1}{2}$ in. thick separated by 3/4 in. lucite strips for the windows.

Essentially the same system of plumbing and purifying was employed separately for the wide- and narrow-gap chambers. Both types of chambers contained the same gas mixture of 90% neon and 10% helium and were maintained at a positive pressure approximately equivalent to 0.2 in. of mineral oil. Purification of the chamber gas was accomplished in a recirculating system by pumping the gas over heated calcium, and through a molecular sieve, submerged in liquid nitrogen, at the rate of approximately 4 ft.^{3} per hour.

Each of the wide-gap chambers was pulsed by an 8-stage Marx generator normally operating at 13 kv. with 3900 pf. per stage. With such a pulsing device the potential drop developed across the 8 in. gap was about 100 kv. The Marx generator itself was triggered by a Science Accessories pulser operating at about 12 kv. The narrow-gap chamber was pulsed by a Berkeley spark gap device which in turn was also triggered by a Science Accessories pulser. With the above arrangements there was a

delay of approximately 150 nsec. between an event trigger and the actual firing of the chambers.

As mentioned previously the spark chambers were photographed by two cameras, each camera viewing one of two 90 degree views of the chambers. The image of the three spark chambers was reduced, by means of an arrangement of front surface mirrors, to fit on 35 mm. film with a resulting demagnification of approximately 60:1. High speed Flight Research cameras, equipped with 125 mm. focal length lenses and Eastman Kodak tri-x film were used. The f stop setting was normally f/8 or f/11. A number of reference fiducials on the chambers were photographed for each event as well as various coded information, via neon data lights. Operation of the spark chambers and the optics system as described above resulted in a spark (track) width of nominally 40 microns on the film.

C. Liquid Hydrogen Target

The liquid hydrogen target, the general features of which are shown in Fig. 2, was of more or less standard design. The inner vessel was constructed of stainless steel, had a diameter of approximately 81 in., a vertical height of 32 in. and a capacity of 2000 liters. In order to minimize interactions in the material of the inner vessel itself, its hemispherical domes were only .050 in. thick. The close fitting vacuum jacket was constructed of

FIGURE 2. General features of the liquid hydrogen target.

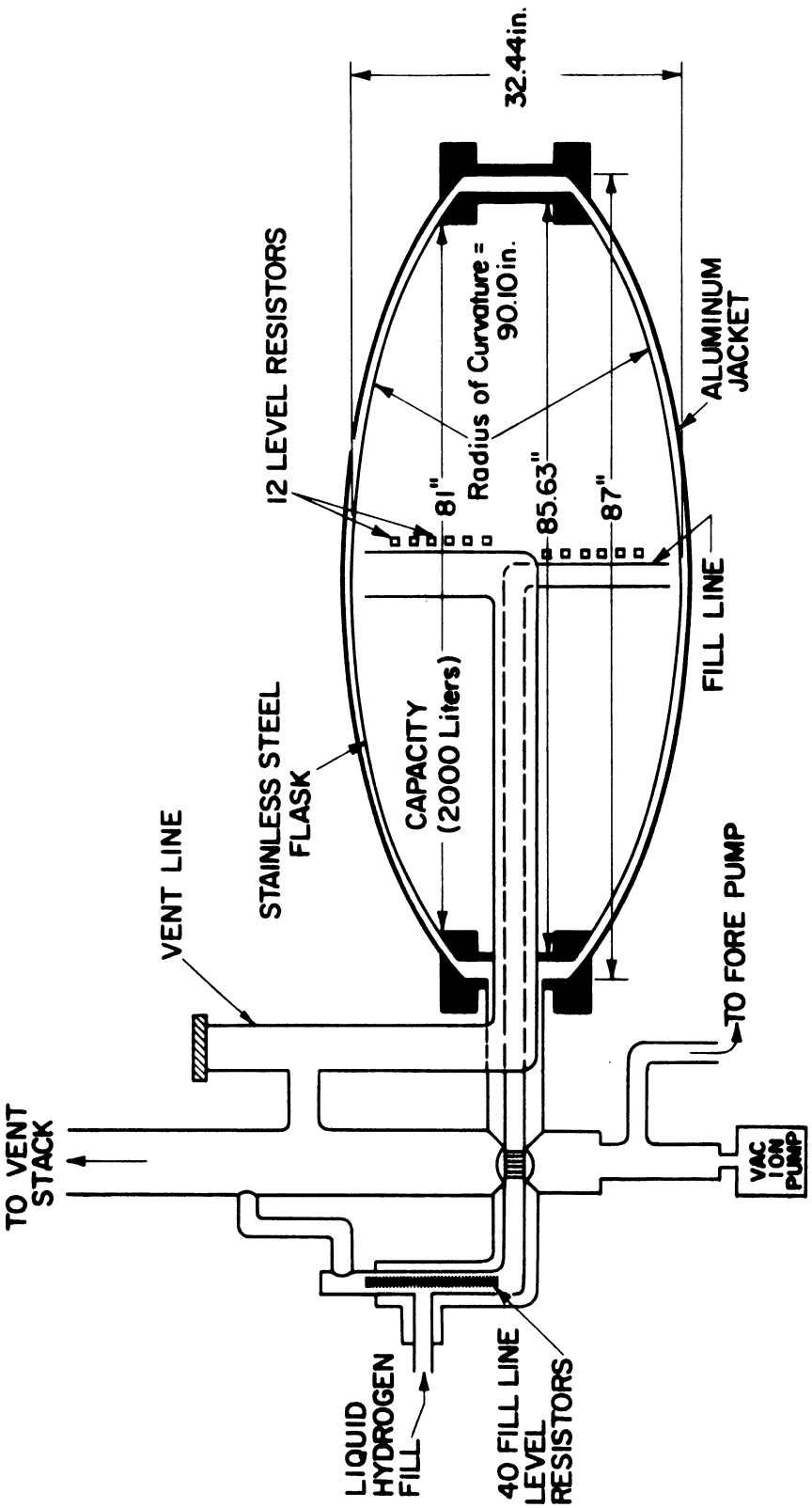
32.44in.
12 LEVEL RESISTORS
Radius of Curvature = 90.10 in.
ALUMINUM JACKET
81"
85.63"
87"
FILL LINE
STAINLESS STEEL FLASK
CAPACITY (2000 Liters)
VENT LINE
TO FORE PUMP
TO VENT STACK
VAC ION PUMP
LIQUID HYDROGEN FILL
40 FILL LINE LEVEL RESISTORS

aluminum and had a dome thickness of 0.25 in. The associated plumbing consisted essentially of a fill line, vent line, associated vacuum system, and a vent stack extending up through the roof of the laboratory. In order to maintain the liquid hydrogen and minimize the boil off rate a vacuum of 10^{-7} mm. Hg. was maintained in the region between the inner vessel and the vacuum jacket and, in addition the inner vessel was heat shielded by twenty wrappings of super insulation. A fore pump was used to bring the vacuum to about 10^{-2} mm. Hg. and a vac ion pump then used to lower it to 10^{-7} mm. Hg. and maintain it at that pressure. A check valve at the top of the vent stack was set to positively pressurize the inner vessel at 0.5 p.s.i. With the above arrangement the boil off rate remained constant at approximately 65 liters per day. At this boil off rate, within 10 days the volume of liquid had dropped to about 2/3 of capacity and the target was refilled.

The level of liquid in the target was monitored by means of two resistor strings. One string of twelve resistors spaced $3\frac{1}{4}$ in. apart and located inside the inner vessel was monitored during normal running. These resistors were calibrated as to spatial location against another string of forty, more closely spaced resistors located in the fill line. The upper thirty of these resistors were separated by 5/16 in. and the lower ten by 10/16 in. The resistors used had resistances of 100 ohms which changed by about 30% when submerged in the liquid hydrogen.

Because of the potential hazards involved with the use of liquid hydrogen, rigid safety procedures were followed throughout the hydrogen run. Standard operating procedure was to have at least one qualified operator with the equipment 24 hours a day and at least one backup man readily available in the vicinity. Several safety devices were built into the experiment, including an alarm system which facilitated an electrical power dropout and started fans to change the air in the experimental building, target heaters for rapid dumping of the target, a flame quenching device for fires at the top of the vent stack, and an emergency power generator. A concentration of 4% hydrogen in an atmosphere is considered to be potentially explosive. With this in mind the alarm system was set to sound off if the concentration, as detected by two sensing devices, reached 20% of 4%. As it turned out the liquid hydrogen target proved to be a trouble free system and worked well throughout the entire hydrogen run.

D. Electronics

Block diagrams illustrating the arrangement of the electronics for the experiment are given in Figs. 3 and 4. The development of the muon and hadron triggers through the Chronetics fast logic is given in Fig. 3. Fig. 4 illustrates the remaining features beyong the Chronetics logic.

FIGURE 3. Electronics block diagram showing the arrangement of the muon and hadron triggers.

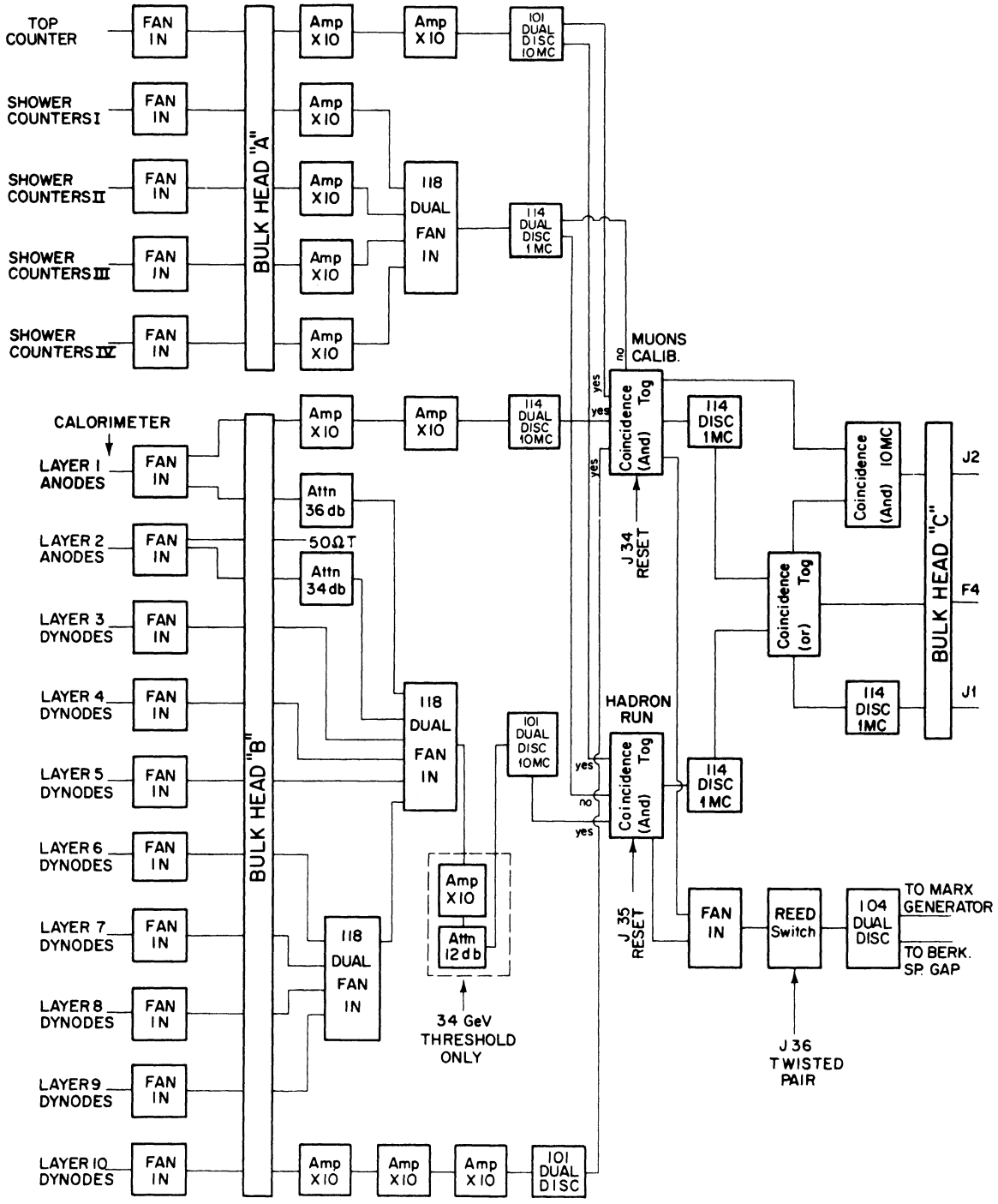
TOP COUNTER
SHOWER COUNTERS I
SHOWER COUNTERS II
SHOWER COUNTERS III
SHOWER COUNTERS IV
CALORIMETER
LAYER 1 ANODES
LAYER 2 ANODES
LAYER 3 DYNODES
LAYER 4 DYNODES
LAYER 5 DYNODES
LAYER 6 DYNODES
LAYER 7 DYNODES
LAYER 8 DYNODES
LAYER 9 DYNODES
LAYER 10 DYNODES
FAN IN
BULK HEAD "A"
BULK HEAD "B"
Amp X10
Attn 36 db
50Ω T
Attn 34 db
Attn 12 db
118 DUAL FAN IN
101 DUAL DISC 10MC
114 DUAL DISC 1MC
114 DUAL DISC 10MC
101 DUAL DISC
34 GeV THRESHOLD ONLY
MUONS CALIB.
HADRON RUN
Coincidence (And) Tog
114 DISC 1MC
J 34 RESET
J 35 RESET
Coincidence (And) 10MC
Coincidence Tog
Coincidence (or)
BULK HEAD "C"
J2
F4
J1
REED Switch
104 DUAL DISC
TO MARX GENERATOR
TO BERK. SP. GAP
J 36 TWISTED PAIR
yes
no

FIGURE 4. Electronics block diagram showing the calorimeter read-out electronics and additional features following the triggering arrangement.

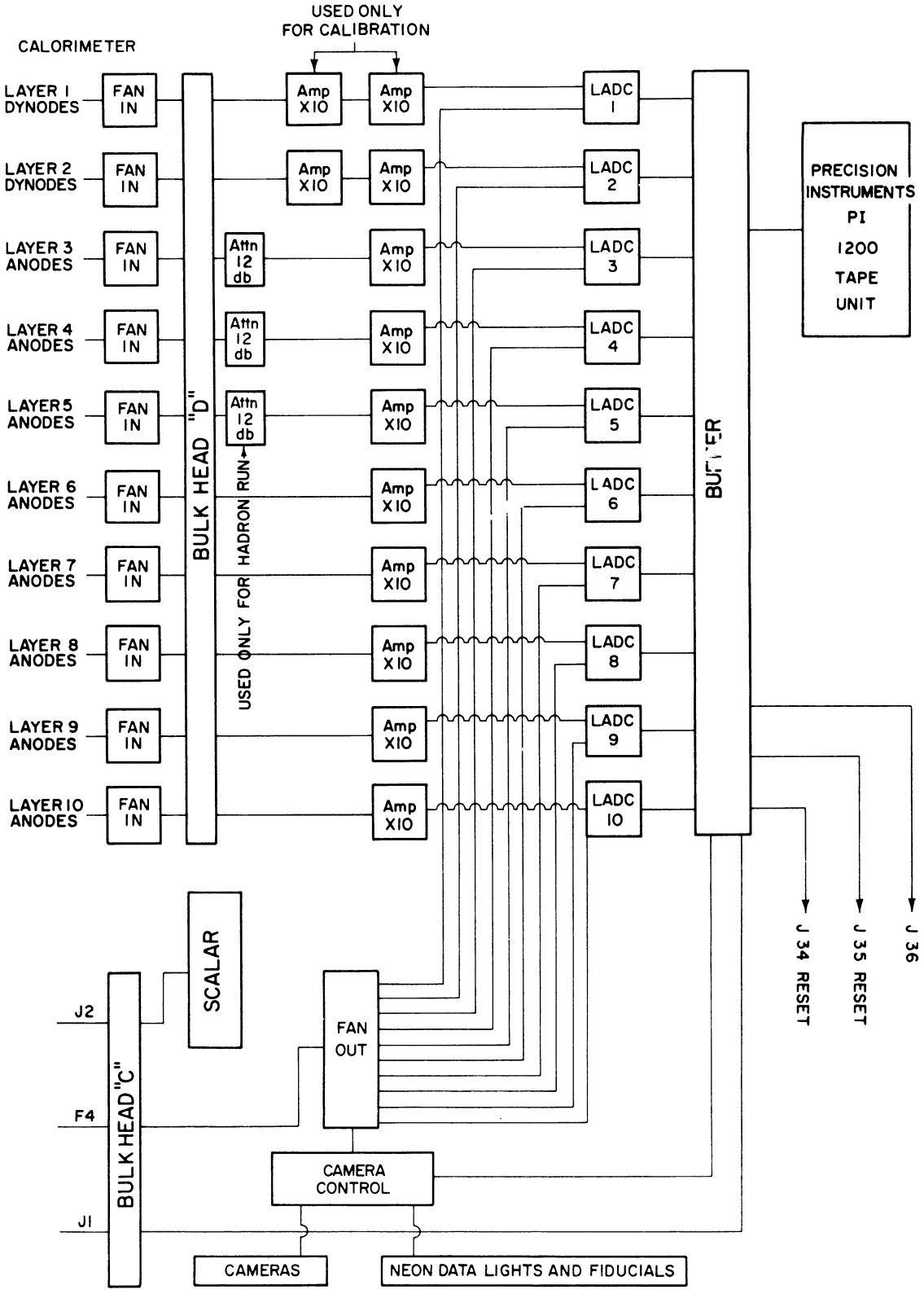
USED ONLY
FOR CALIBRATION
CALORIMETER
LAYER 1
DYNODES
LAYER 2
DYNODES
LAYER 3
ANODES
LAYER 4
ANODES
LAYER 5
ANODES
LAYER 6
ANODES
LAYER 7
ANODES
LAYER 8
ANODES
LAYER 9
ANODES
LAYER 10
ANODES
FAN IN
BULK HEAD "D"
Amp X10
Attn 12 db
USED ONLY FOR HADRON RUN
LADC 1
LADC 2
LADC 3
LADC 4
LADC 5
LADC 6
LADC 7
LADC 8
LADC 9
LADC 10
BUFFER
PRECISION INSTRUMENTS PI 1200 TAPE UNIT
J 34 RESET
J 35 RESET
J 36
SCALAR
FAN OUT
J2
F4
J1
BULK HEAD "C"
CAMERA CONTROL
CAMERAS
NEON DATA LIGHTS AND FIDUCIALS

A total of 112 photomultiplier tubes were employed in the experiment; 8 for the top counter, 8 for each of the 10 layers of the calorimeter, and 24 for the shower counters. RCA type 6810 photomultipliers were used for the top counter, layers 1 and 2 of the calorimeter and the shower counters, while EMI 9816's were used for the remaining layers of the calorimeter. The output from the top counter and each layer of the calorimeter was then the summed output of 8 photomultipliers. The 24 shower counters were divided into 4 equal groups, with the output of the counters in each group taken together to give a summed output for each group.

Three modes of triggering were available: the normal charged hadron trigger, a muon trigger for equipment testing and calibrations, and a trigger for neutral particles. The charged hadron trigger, as shown in Fig. 3, consisted of a 3-fold coincidence between the top counter, the calorimeter, and the shower counters as an anti-coincidence. The muon trigger consisted of a 4-fold coincidence between the top counter, layer 1 and layer 10 of the calorimeter, and the shower counters as an anti-coincidence. From the calorimeter, the photomultiplier dynodes were used for the trigger and the anodes for the LADC input. The exceptions were layers 1 and 2 where just the reverse was true. The desired energy threshold for the trigger was achieved by appropriately attenuating the pulse from each layer

and then discriminating the resultant summed pulse from all layers. As indicated in Figs. 3 and 4, bulk head "C" can be referred to as the output from the Chronetics fast logic. F4 goes to a fan-out which distributes the trigger to the LADC gates and the camera control circuit. J2 was used to supply the trigger for the test scaler. Furthermore, the Chronetics fast logic also supplied the trigger for the spark chambers and the required holdoffs.

The following comments should be made, regarding the function of the LADC's and the buffer. In simple terms an LADC for a given calorimeter layer looked at the summed photo-multiplier output pulse, for a given event, for that layer and in turn supplied a "channel number" from 1 to 128 which was linearly proportional to the log of the pulse. The LADC's output went to the buffer which coded the output "channel number" for each layer in terms of 8 bits of information. Any "channel number" from 1 to 127 was coded in terms of 7 bits and "channel number" 128 was coded in terms of the 8th bit and represented an overflow. The 8-digit octal event number was represented in terms of 24 bits, and the 2 digit octal run number by 6. In addition, there were 6 more bits of coded information as output from the buffer. The LADC (calorimeter) information as well as the coded information was written on magnetic tape and also visually displayed for each

event. After the buffer had recorded the above information it signalled its readiness for another event by resetting the Chronetics coincidence unit and camera control circuit.

E. Ionization Calorimeter

Grigorov, et al.[20] first suggested the use of the ionization calorimeter for measuring the energy of strongly interacting particles. Use of ionization calorimeters is based on the principle that the incident particle will convert its energy into ionization loss in the dense material of the calorimeter. This conversion is accomplished via the cascading of hadron interactions in which neutral pions are produced. These neutral pions decay into gamma rays which initiate the electromagnetic or soft cascades. If a sufficient amount of absorber material is provided, virtually all the energy of the incident particle will be converted into ionization with only a small fraction of the energy being carried away by fast muons and neutrinos. The energy of the incident particle is then determined by sampling the ionization loss at various depths in the absorber with suitable detectors. A comprehensive discussion of the principles and design of ionization calorimeters is given by Murzin[21].

The calorimeter used in this experiment had a cross-sectional area of 8 x 8 ft.^{2} and a thickness of iron corresponding to 1130 gm/cm.^{2}. The iron stack was striated with 10 layers of

plastic scintillator labeled T1 through T10 in Fig. 1 and located at respective depths of 40, 120, 210, 330, 450, 570, 690, 810, 970 and 1130 gm./cm.^{2}. As mentioned previously each layer was viewed by 8 photomultiplier tubes which summed together gave an output pulse as a measure of the ionization at that layer. It should be noted that all the photomultiplier tubes were individually examined as to linearity and that the tubes were operated at voltages well within their linear range of operation.

According to Lyon and Subramanian[22], when scintillators are used as detectors in an ionization calorimeter, the measured energy of an incident hadron can be expressed by

$$E = \int\int \epsilon(\beta)\, N(\beta, t)\, dt d\beta$$

where $N(\beta, t)$ is the number of particles with specific ionization β at thickness t, and $\epsilon(\beta)$ is an efficiency factor for response to specific ionization, with $\epsilon(\beta) = 1$ at $\beta = \beta$ minimum. For a finite number of probes separated by thicknesses of absorber the integral is replaced by a sum over the number of layers. For the interactions reported in this paper, the energy was calculated from

$$E = \frac{f_i \beta}{\cos\theta}\left[\frac{N_1}{2} X_1 + \sum_{i=2}^{L} \frac{N_{i-1} + N_i}{2} X_i + \wedge N_L\right] \qquad \text{(II. 1)}$$

where N_i is the equivalent number of particles with specific

ionization β, f_i is a factor (specified later) to account for unsampled energy losses, and $\cos\theta$ is the direction cosine for the beam particle's trajectory, to correct the thickness traversed. The last term

$$\Lambda N_L = \int_0^\infty e^{-X/\Lambda} N_L dX$$

represents an extrapolated area of the shower curve beyond the last probe, L, traversed by the extrapolated trajectory of the beam particle. It has been assumed that exponential absorption prevails at large thicknesses. The attenuation length Λ was chosen from a study of the calorimeter to be 240 gm/cm^{-2}.

The calorimeter was calibrated in terms of cosmic ray muons, that is, N_i represents the number of "equivalent muons" at the i^{th} layer. These muons have on the average specific ionization, β. In essence N_i was a measured quantity, being given by the ratio of the pulse height in the i^{th} layer to the average muon pulse height. Periodic calibrations (to be discussed later) were taken to determine the average muon pulse height at each layer. At Echo Lake the muon flux is dominated by muons of about 2 GeV. A 2 GeV muon, in traversing iron loses energy at the rate of 1.72 $MeV\text{-}gm^{-1}\text{-}cm^2$. Since the muon calibration is dominated by muons having energies of about 2 GeV, a value of $\beta = 1.7 \times 10^{-3}$ $GeV\text{-}gm^{-1}\text{-}cm^2$ was chosen to be used in equation (II. 1).

The problems involved with unsampled energy losses in ionization calorimeters are not completely understood. There are, however, three effects which should be mentioned as contributing factors to this unmeasured energy. First and most significant is the unsampled energy going into nuclear disentegrations, the products of which are sampled by the scintillators with low efficiency. Secondly, there is the so-called transition effect, as discussed by Pinkau[23], which occurs because the absorption and regeneration properties of the probes are different from those of the absorber. This effect is dependent on the thickness of the scintillators. Thirdly, there is the possibility of energy escaping from the bottom and sides of the calorimeter, both as E. M. showers and as muons and neutrinos. Using Monte Carlo techniques, W. V. Jones[24] has recently studied the first and the third of the above mentioned effects. It should be pointed out that equation (II. 1) is essentially the same as that used by Lyon and Subramanian[22] in studying a calorimeter of similar design operated at Echo Lake in 1967. In that study a value of f = 1.3 was chosen to correct for the unsampled energy. The energy resolution of the calorimeter was also studied by these authors and estimated to be $\pm$ 20%.

In view of the above discussion, and communication with D. E. Lyon[25], values of f_i to be used in equation (II. 1) were chosen

to be

$f_i = 1.3$ $\quad i = 1, 2, 10$ $\quad$ (scintillators = 3/4 in. thick)
$f_i = 1.4$ $\quad i = 3\text{-}9$ $\quad$ (scintillators = $1\frac{1}{2}$ in. thick)

as a correction to the energy determination to account for unsampled energy losses.

In concluding the discussion of the calorimeter, it is of interest to make some additional comments regarding the calibration procedures. For simplicity the following remarks are made with reference to the i^{th} layer of the calorimeter and it should be kept in mind that each of the 10 layers were calibrated in the same manner. An LADC calibration and a muon calibration were taken weekly in order to relate the number of "equivalent muons" (N_i) to the pulse height (V_i) produced by a hadron event. For the LADC calibration a fixed pulse was attenuated and supplied to the LADC in 5dB steps, resulting in a plot of dB vs channel number. For the muon calibration the system was triggered on muons. The pulse from each muon (V_{μ_i}) was amplified by an amount A_i and supplied to the LADC. Triggering on 1500 muons resulted in a distribution of channel numbers with the median channel number being chosen as the channel number corresponding to an average muon pulse ($\overline{V}_{\mu_i}$) when amplified an amount A_i. The attenuation (dB'_{μ_i}) corresponding to this amplified average muon pulse is supplied by the LADC calibration and the attenuation corresponding to the average muon pulse unamplified is then

$$dB_{\mu_i} = dB'_{\mu_i} + A_i \quad .$$

The number of equivalent muons is just

$$N_i = V_i / \overline{V}_{\mu_i}$$

which when expressed in terms of attenuation becomes

$$\log N_i = \frac{dB_{\mu_i} - dB_i}{20}$$

where dB_i is the attenuation corresponding to the LADC channel number resulting from V_i. Rewritting further using

$$6.02 = 20 \log 2$$

and defining

$$T_i \equiv \frac{dB_{\mu_i} - dB_i}{6.02}$$

yields

$$N_i = 2^{T_i}$$

which was the equation used to determine the number of "equivalent muons" for the i^{th} layer, for a given hadron event. It may be of interest that in terms of the number of minimum ionizing particles, the energy threshold for triggering corresponded to

$\Sigma N_i \geq 300$ particles for the 85 Gev threshold and $\Sigma N_i \geq 120$ particles for the 34 Gev threshold.

Shown in Fig. 5 are the average shower curves for nine energy bins. These shower curves, produced from our experimental data on approximately 50,000 charged hadrons which did not interact in the target, exhibit the calorimeter behavior in terms of number of minimum ionizing particles as a function of depth in the calorimeter. The shower curves for the hadrons which interacted in the target exhibit the same general behavior, but were derived from much smaller statistics, and have not been shown.

FIGURE 5. Calorimeter average shower curves for nine energy bins.

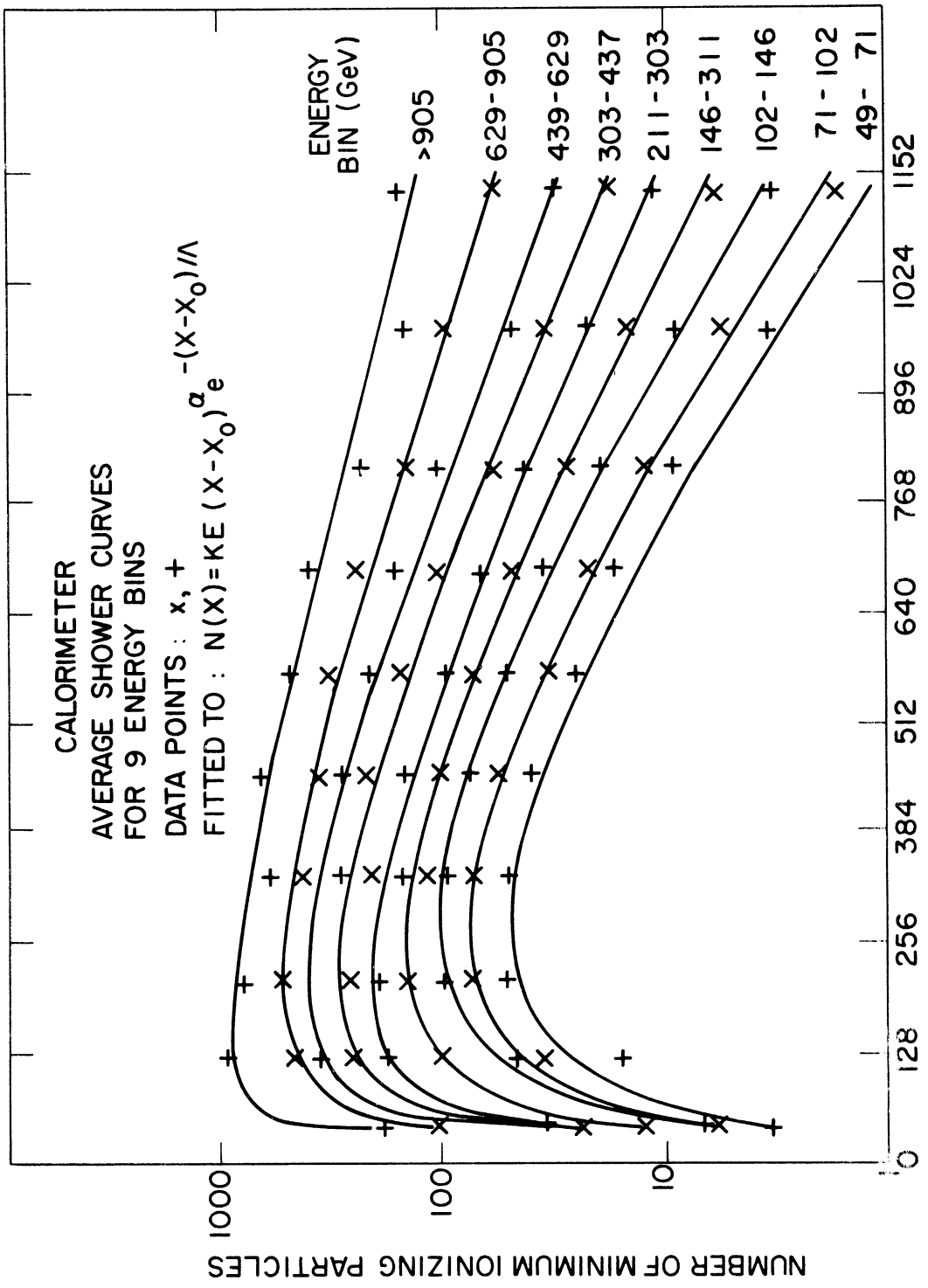
CALORIMETER
AVERAGE SHOWER CURVES
FOR 9 ENERGY BINS
DATA POINTS : x, +
FITTED TO : $N(X)=KE\,(X-X_0)^{\alpha}e^{-(X-X_0)/\Lambda}$
ENERGY BIN (GeV)
>905
629-905
439-629
303-437
211-303
146-311
102-146
71-102
49-71
NUMBER OF MINIMUM IONIZING PARTICLES
1000
100
10
0
128
256
384
512
640
768
896
1024
1152
DEPTH IN CALORIMETER
(gm/cm² of Fe)

CHAPTER III

DATA ANALYSIS

In operating the experiment from March, 1968 to May, 1969 a total of 30,000 charged hadron triggers were collected using the carbon target and 116,000 triggers with the liquid hydrogen target. Presented in this chapter is a discussion of the data analysis procedures applied in selecting interactions from the above triggers. Specifically discussed are the scanning and measuring procedures, the reconstruction and optical correction methods, the fiducial volume for acceptance, the corrections for delta rays and the data organization for physics analysis. Specific physics analysis and any further biases and corrections regarding the interactions will be discussed in the final chapter.

A. Scanning and Measuring

The corresponding pictures from each of the two stereo views were simultaneously scanned for events showing a single track in the upper wide-gap spark chamber and two or more associated tracks in the lower wide-gap chamber. These selected interactions were coded as to event number and number of tracks per view in the lower chamber. Because of associated delta ray production, events showing only two or three tracks in the lower chamber

had additional comments as to any bending of these tracks and their visible depth of penetration into the narrow-gap iron plate chamber. For all interactions, when counting the number of tracks in the lower chamber, tracks showing scatters at the center foil or wiggles were assumed to represent delta rays and were not counted.

The interactions were digitized at the University of Wisconsin and put directly on magnetic tape. The carbon interactions were measured on an image plane digitizer having a least count of 6 microns on the film. The hydrogen interactions were measured on a film plane digitizer having a least count of 1 micron on the film. In each view of every interaction, four reference fiducials, the upper chamber track and all counted tracks in the lower chamber were digitized. Sixteen points were digitized along each track.

B. Event Reconstruction and Optics Corrections

Each interaction was spatially reconstructed to the following extent. The track of the incoming or beam particle was parameterized as to direction cosines and coordinates. The secondary particles were each assigned an angle relative to the beam direction in each of the two projected systems corresponding to the two stereo views. And, the coordinates of the interaction vertex were determined.

The beam track was reconstructed by tracing "light rays" from the measured points on the film back through the optical system into the chambers, and then performing a non-linear least squares fit of the reconstructed light rays to a function of the sum of the squared distances between the light rays and the fitted track. Specifically the function

$$\chi^2 = \sum_{i=1}^{N} \left(\frac{d_i}{\sigma} \right)^2$$

was minimized, where N was the number of measured points, σ was the resolution, and d_i was the distance of the i^{th} ray from the fitted track. The functional form of d_i is that of the distance between the two skew lines in space, that is

$$\begin{aligned} d_i = \{ & (X_i - X)(\cos \beta_i \cos \gamma - \cos \gamma_i \cos \beta) \\ & + (Y_i - Y)(\cos \gamma_i \cos \alpha - \cos \alpha_i \cos \gamma) \\ & + (Z_i - Z)(\cos \alpha_i \cos \beta - \cos \beta_i \cos \alpha) \} \; / \; \sin \theta_i \end{aligned}$$

where

$$\cos \theta_i = \hat{X}_i \cdot \hat{X}$$

and

$$\hat{X}_i = \hat{X}_i (\alpha_i, \beta_i, \gamma_i, X_i, Y_i, Z_i)$$

for the i^{th} ray

with

$$\hat{X} = \hat{X}(\alpha, \beta, \gamma, X, Y, Z)$$

for the fitted track.

It should be mentioned that no attempt was made to correlate the tracks of the reaction products in the two orthogonal views so that only projected angles of the charged secondaries relative to the beam were obtained in each view. However, a re-conical projection of these angles was made so that the projected angles were known in a plane containing the incident "beam" particle. This was performed with the knowledge of the optical system and the real-space reconstructed parameters of the incident particle in the upper wide-gap chamber.

The interaction vertex was determined by least squares fitting the upper chamber track and each of the tracks of the charged particles in the final state to the vertex, parameterized as X_I, Y_I, Z_I. In making the fit to the vertex, the information from both of the projected systems was simultaneously used to provide the best fit. The resolution in vertex determination was $\pm$ 1.0 cm. in Z_I and $\pm$ 0.2 cm. in X_I and Y_I.

Prior to reconstruction, each measured point was transformed and corrected based on predetermined optics parameters. The method applied in determining these parameters was to fit a fiducial plate containing 32 equally spaced fiducials and 8

fiducials on the chamber. The general procedure was to form χ^2, a function of the parameters, and then minimize it with respect to these parameters. χ^2 was of the form

$$\chi^2 = \sum_i \left\{ \left(\frac{U_i - Y_i}{\sigma_{iy}} \right)^2 + \left(\frac{V_i - Z_i}{\sigma_{iz}} \right)^2 \right\}$$

where the summation was over the number of iiducials, and U_i, V_i were the assigned coordinates of the i^{th} fiducial in the chamber reference system. Y_i, Z_i were the measured coordinates of the i^{th} fiducial after transformation from the encoder frame through the optics system, to the same reference frame as that of U_i, V_i. σ_{iy}, σ_{iz} were the measuring errors associated with the i^{th} fiducial and consisted of the errors in specifying U_i, V_i as well as measurement errors. The correction parameters then entered χ^2 via the Y's and Z's of the fiducials. The correction functions for Y and Z were taken to be of the form

$$fY = F_1 Y + F_2 Z + F_3 Y^2 + F_4 YZ + F_5 Z^2$$

$$fZ = G_1 Y + G_2 Z + G_3 Y^2 + G_4 YZ + G_5 Z^2$$

where the F's and G's were parameters to be determined. Further formulation in terms of additional parameters, such as magnification and translation parameters, was completed as Y and Z were transformed into the same reference frame as that of the assigned

fiducial coordinates U and V. The actual minimization of χ^2 was done by a University of Wisconsin Computer Center library routine called Gaushaus. It provided a least squares estimate of the parameters using an iterative technique in which the estimates at each interaction were obtained by a method which combined the Taylor series method and the method of steepest descent.

C. Fiducial Volume for Acceptance

The fiducial volume for acceptance of events for analysis was chosen such that the extrapolated trajectory of the beam track was restricted to pass within the top counter, within 1.4 cm of the edges of layer 2 and within 11.9 cm of the edges of layer 8 of the calorimeter. Interactions involving the liquid hydrogen target were further restricted to require the interaction vertex to be at least 1.0 cm. in from the vessel walls. No such restrictions as to location of the vertex in the target volume were necessary for the carbon target as there was no other material in its immediate vicinity. Further restrictive cuts as to acceptance yielded no change in energy or multiplicity dependent quantities for either the carbon or liquid hydrogen targets.

D. Delta Rays

Delta ray production was a problem in this experiment in that a charged hadron traversing the target would, in a fraction

of the triggers, produce one or more associated delta rays and simulate an interaction. The simulation of a 2-prong interaction was the most prevelant, due to the production of usually only one delta ray. The delta rays produced with low energy were easily rejected as their tracks in the lower wide-gap spark chamber appeared wiggly or showed a scatter at the center foil. Low energy in this context refers to the delta rays having energies of the order of 50 MeV or less. That is, the mean Coulomb scattering angle of a 50 MeV delta ray which has traversed a 0.002 in. aluminum foil is 0.5 degree, essentially the minimum scattering angle resolved on the scanning table. Genuine 2- and 3-prong interactions were distinguished from simulated interactions, due to the production of higher-energy delta rays, by observing the depth of penetration of each of the tracks into the narrow-gap iron plate chamber. It was assumed that tracks associated with a strongly interacting particle would be observable down to the lowest gap of the iron plate chamber, but that this would not hold true for delta rays. This assumption was based on the comparative range energy relations of strongly interacting produced secondaries, assumed to be mainly pions, to that of electrons and on the probability of producing a delta ray (electron) of energy greater than E.

An estimate of the number of delta rays expected to penetrate to various depths in the iron plate chamber may be made using the

result as given by D. M. Ritson[26].

$$N = \frac{0.15}{\beta^2} \frac{Z}{A} \frac{z^2 X}{E}$$

where E is in MeV and N is the number of delta rays produced with energy greater than E by a particle of charge z and velocity βc in traversing a material with $\frac{Z}{A}$ and thickness X gm/cm^2. The energy, E_i, necessary for an electron to penetrate into the i^{th} gap was estimated from the amount of material the electron would have to traverse and the curves given by Ritson[26] for the mean range of electrons. The thickness of the carbon target was 17.78 gm/cm^2 and the average thickness of the hydrogen target, including vessel, was 9.67 gm/cm^2. β^2 was taken to be 1.0 for relativistic particles. Table III-1 gives the comparison between the number of predicted and observed delta rays able to penetrate into the 1^{st}, 2^{nd}, and 3^{rd} gaps of the iron plate chamber. In this table, N_t is the total number of particle traversals, E_i is the energy required for a delta ray to penetrate to the i^{th} gap, and N_i is the number of delta rays produced per particle traversal with $E > E_i$.

TABLE III-1

Comparison of Observed and Predicted Delta Rays

Target	Gap	E_i(MeV)	$N_i(\times 10^{-2})$	Number Predicted	Number Observed
Hydrogen	1	76	1.330	864	437
N_t = 65,000	2	586	.172	112	107
	3	4890	.021	14	31
Carbon	1	79	1.660	227	120
N_t = 13,700	2	590	.225	31	25
	3	4860	.027	4	4

It is seen that the agreement is good for gaps 2 and 3. The disagreement for gap 1 is largely due to an observed inefficiency for sparking in that gap. In terms of the removal of simulated interactions, tracks which did not continue beyond the 3rd gap were assumed to be associated with delta rays. Of the events scanned which showed two straight tracks in the lower wide-gap spark chamber, 13% and 18% remained after delta ray subtraction as genuine 2-prong interactions in the carbon target and hydrogen target, including vessel, respectively.

Also investigated was the production of delta rays by the final state charged particles. Based on the observations of events showing two straight tracks in the lower wide gap chamber, the probability, per average particle traversal, of producing a delta ray whose track appeared straight was found to be equal to 0.03. An average particle traversal was defined as the traversal of a charged hadron through the entire target. Knowing this probability

and assuming that on the average the produced particles would traverse one-half of the target, it was possible to determine the probability of producing a delta ray for each multiplicity. This information was then applied to investigate a possible bias to the charged multiplicity distributions and to correct the average charged multiplicity.

E. Data Organization

As each event was reconstructed, its energy information was incorporated, and an output tape containing the necessary information for analysis was written. For the hydrogen data it was necessary to update this tape, incorporating the hydrogen level information for each event.

For analysis purposes, the events were grouped as to energy in bins approximately $\pm$ 20% wide. The bins were: 34-49, 49-71, 71-102, 102-146, 146-211, 211-303, 303-437, 437-629, 629-905 and $\geq$ 905 GeV.

It was found that threshold effects of the calorimeter were important up to an energy value approximately double the threshold setting. Because of these effects the useful data for analysis was required to have energy values of $E \geq 71$ GeV for the 34 GeV threshold and $E \geq 146$ GeV for the 85 GeV threshold. Above 146 GeV the data from both thresholds could be combined. In presenting the data on average charged multiplicity and charged multiplicity

distributions the interactions in the energy bins 71-102 and 102-146 GeV were combined.

As a point of interest, presented in Table III-2 is a summary of event rejection because of threshold effects and cuts made on the fiducial volume.

TABLE III-2

Summary of event rejection for fiducial volume of acceptance and threshold effects. The numbers pertain to interactions having three or more charged tracks in the final state

HYDROGEN

	Number of Events	Accumulative Fraction of Acceptance
Number of observed interactions	2228	
Number rejected because of geometry cut	808	.64
Number rejected because interaction vertex was not in hydrogen	614	.36
Number rejected because of threshold effects	232	.26
Number of events remaining for analysis	574	

CARBON

Number of observed interactions	696	
Number rejected because of geometry cut	261	.63
Number rejected because interaction vertex was not in carbon	8	.62
Number rejected because of threshold effects	172	.38
Number of events remaining for analysis	255	

CHAPTER IV

RESULTS AND CONCLUSIONS

In this final chapter the results of the analysis are presented and discussed for interactions which satisfied the acceptance criteria. Presented first are the results obtained from fitting the experimental multiplicity distributions of final state charged particles to the prediction of the multiperipheral model of Chew and Pignotti[10] and the models of C. P. Wang[12]. Second, a comparison is made between the average charged multiplicity in hydrogen and carbon. Also presented are the results of fitting the hydrogen data obtaining to average charged multiplicity to the hydrodynamical model of Belenjki and Landau[13], the multiperipheral model of Chew and Pignotti[10], and the isobar-pionization model of Pal and Peters[15]. Third, the angular distributions of the charged particles in the final state are discussed, and the results of fitting those distributions to a C.M. isotropic distribution and to C. M. distributions of the form $A + B \cos^{M}\theta_{c.m.}$ $(A + B = 1,\ M = 2, 4)$ are presented. This is followed by the results obtained in fitting the forward and backward branches of the modified Duller-Walker plots, using the approach of Cocconi[19] to estimate the inelasticity. The conclusions are then summarized.

A. Multiplicity Distributions

The breakdown of the interactions accepted for analysis, as to numbers of observed tracks and energy grouping, is summarized for hydrogen and carbon in Tables IV-1 and IV-2. It is required by the conservation of charge, that an interaction between a charged cosmic ray hadron and a proton in the hydrogen target have an even number of charged particles in the final state. The observation of events with an odd number of charged tracks was attributed to cases where the recoil proton was not emitted into the geometry of the lower wide-gap spark chamber. This supposition about the recoil proton has been supported by the results of Monte Carlo generated events which were required to satisfy the geometry of the experimental arrangement.[25] Table IV-3 gives the modification of Table IV-1, where the number of charged tracks has been increased by one for the events showing an odd number of observed tracks, to account for the unobserved recoil proton. The situation regarding unobserved recoil protons in the case of interactions with the carbon target is unclear because of the presence of neutrons in the carbon nucleus and the possibility of secondary interactions with other nucleons in the nucleus. In light of these complications no attempt was made to adjust Table IV-2 for unobserved recoil protons.

TABLE IV-1

Summary of the Number of Hydrogen Interactions Selected for Analysis

Charged Tracks	Number of Interactions (As Observed) Energy Bin (GeV)				
	71-146	146-211	211-303	303-437	437-905
2	32	38	24	11	2
3	21	35	16	10	4
4	18	23	20	9	10
5	17	28	13	8	4
6	12	29	17	11	5
7	12	23	11	4	3
8	11	16	19	7	4
9	8	12	11	7	3
10	7	11	10	5	1
11	4	10	4	2	3
12	4	5	7	2	
13	2	2	5	2	1
14		4	1	5	1
15	1	3	2	2	1
16					2
17					1
18	1		1		
$\geq$ 19		1			

TABLE IV-2

Summary of the Number of Carbon Interactions Selected for Analysis

Charged Tracks	Number of Interactions (As Observed) Energy Bin (GeV)				
	71-146	146-211	211-303	303-437	437-905
2	7	16	6	2	2
3	13	10	6	4	
4	10	9	9	1	
5	7	11	1		
6	4	18		1	2
7	10	9	7	2	2
8	4	2	8	1	3
9	6	3	6	2	
10	6	9	4		1
11	5	2	2	1	1
12	3	5	1	1	1
13	3	3	2	1	3
14	1	4	2	1	1
15	1	2	2		
16	1	2	1		
17	1	2	2		
18					
19					
20		1		2	1
$\geq$ 21	1	1	1		

TABLE IV-3

Modification of Table IV-1, where the number of charged tracks has been increased by 1 for odd numbers of observed tracks to account for the unobserved recoil proton in these cases.

Charged Tracks	Number of Interactions Energy Bin (GeV)				
	11-146	146-211	211-303	303-437	437-905
2	32	38	24	11	2
4	39	58	36	19	14
6	29	57	30	19	9
8	23	39	30	11	7
10	15	23	21	12	4
12	8	15	11	4	3
14	2	6	6	7	2
16	1	3	2	2	3
18	1		1		1
$\geq$ 20		1			

Shown in Figs. 6 - 9 are the multiplicity distributions of final state charged particles for interactions occurring in the liquid hydrogen. The grouping in terms of energy is indicated on the plots. The experimental points were plotted directly from Table IV-3 with the associated error bars representing the square root of the number of events with a given number of charged tracks in the final state. Also shown on these plots are the best fits to the data according to the predictions of the multiperipheral model and the models of C. P. Wang. A χ^2 fit in terms of two parameters was made to the experimental distributions. The functional forms explicitly fitted have been described in Chapter I. Events showing two charged tracks in the final state were excluded from the fit because of the uncertainties associated with the simulation of 2-prong events due to delta ray production. The values of the fitted parameters for each energy bin and each model are summarized in Table IV-4. In this table $\langle n_c \rangle$ is the average number of charged particles in the final state.

For the hydrogen data, as shown in Figs. 6 - 9, the experimental multiplicity distributions of charged particles in the final state are in good agreement with Wang model I. The prediction of Wang model I, as discussed in Chapter I, is that the distribution of charged secondaries should be Poisson in the number of pairs of produced charged particles, assumed to be mainly

FIGURE 6. Multiplicity distribution of charged particles in the final state for hydrogen events in the energy bin 71-146 GeV.

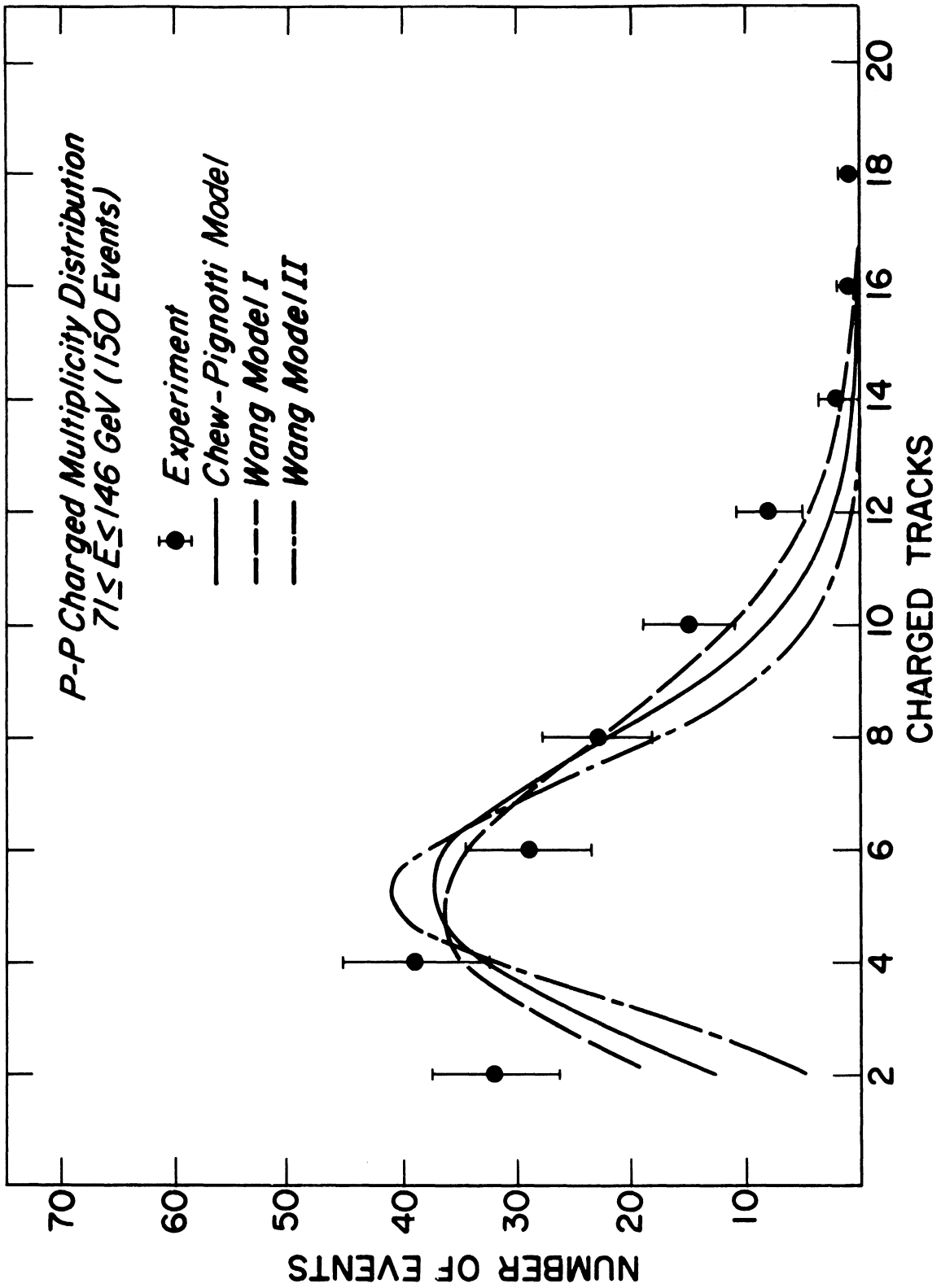
P-P Charged Multiplicity Distribution
71≤E≤146 GeV (150 Events)
Experiment
Chew-Pignotti Model
Wang Model I
Wang Model II
NUMBER OF EVENTS
CHARGED TRACKS
70
60
50
40
30
20
10
2
4
6
8
10
12
14
16
18
20

FIGURE 7. Multiplicity distribution of charged particles in the final state for hydrogen events in the energy bin 146-211 GeV.

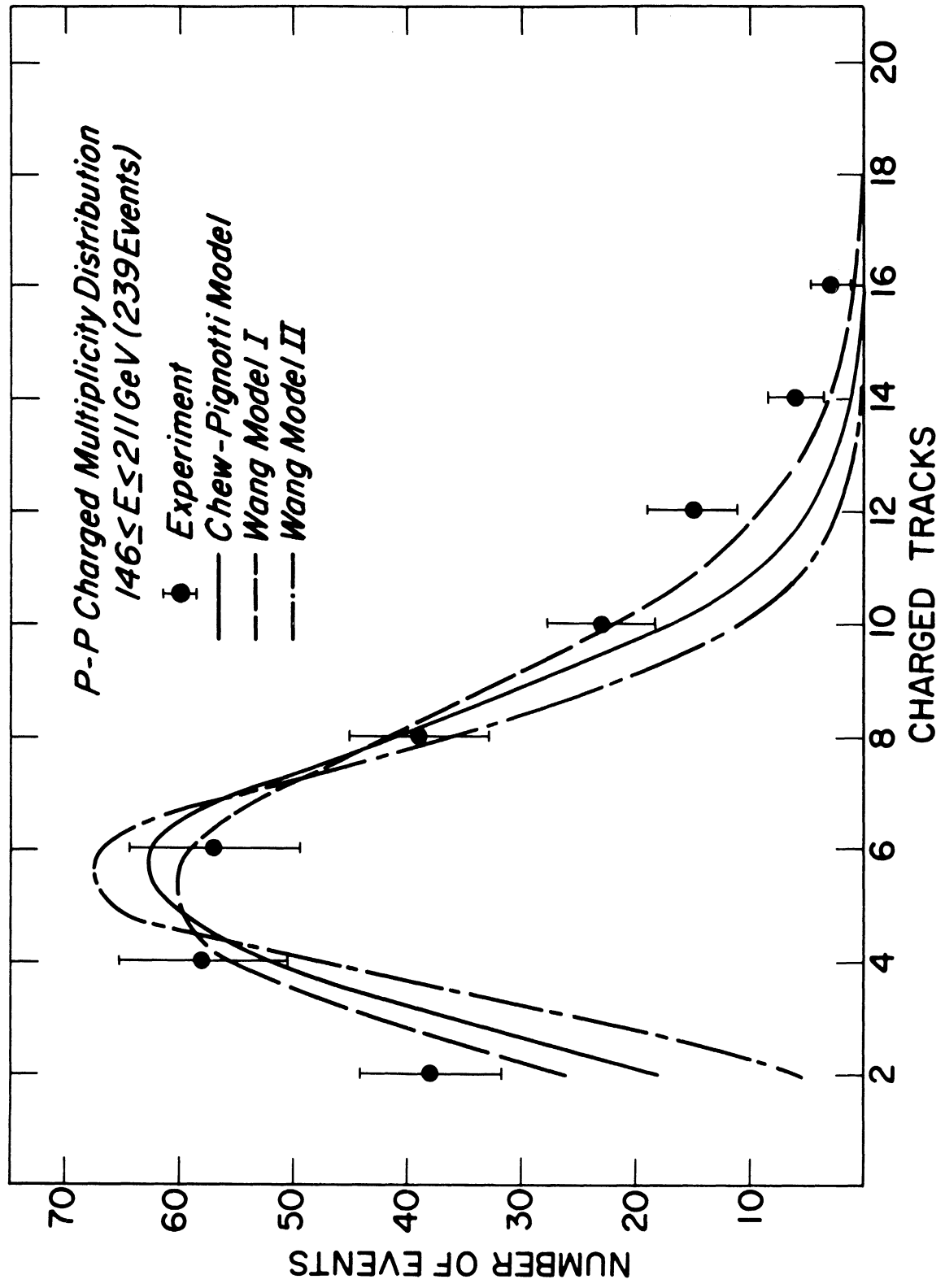
P-P Charged Multiplicity Distribution
146≤E≤211 GeV (239 Events)
Experiment
Chew-Pignotti Model
Wang Model I
Wang Model II
NUMBER OF EVENTS
CHARGED TRACKS
70
60
50
40
30
20
10
2
4
6
8
10
12
14
16
18
20

FIGURE 8. Multiplicity distribution of charged particles in the final state for hydrogen events in the energy bin 211-303 GeV.

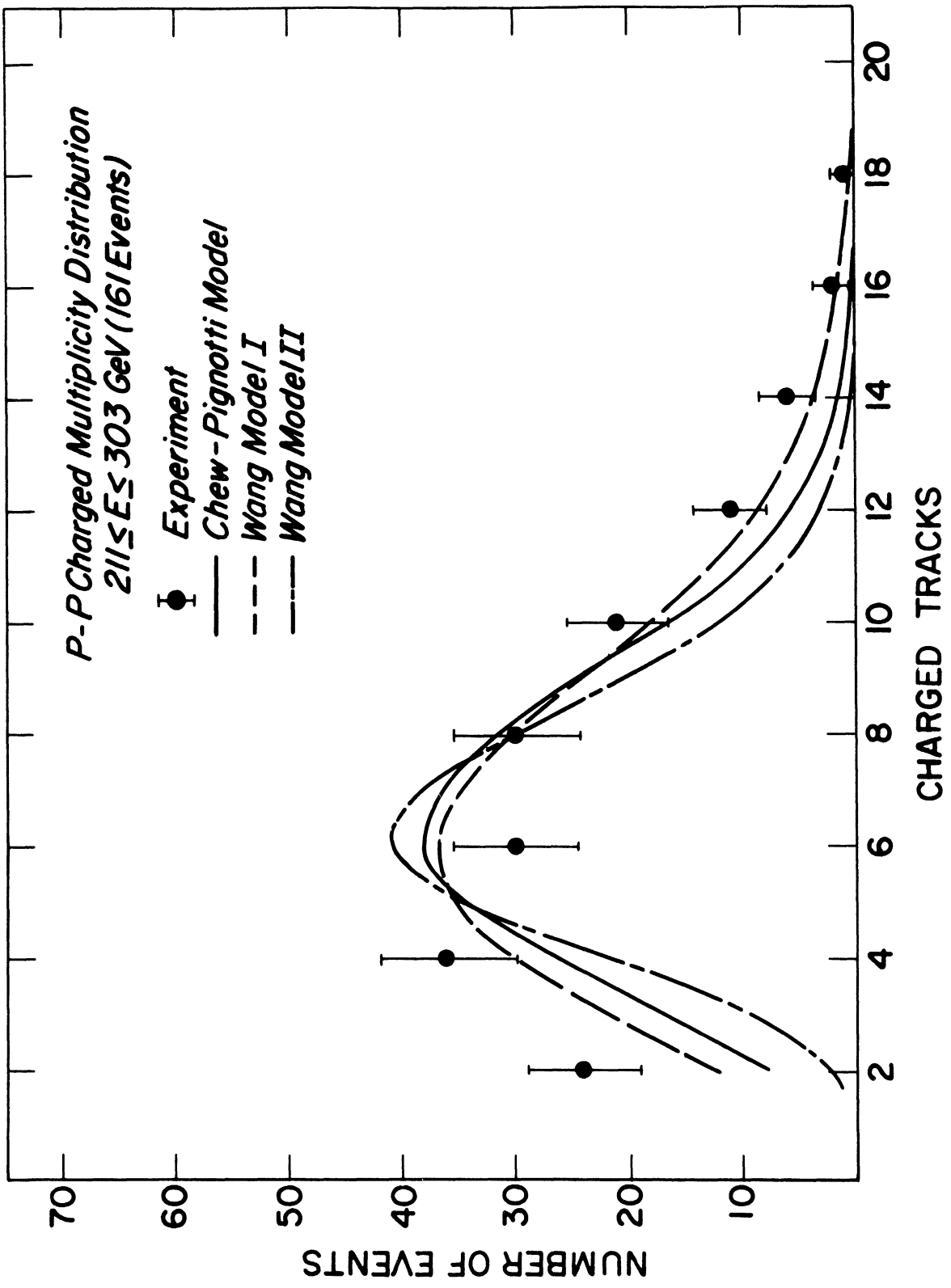
P-P Charged Multiplicity Distribution
211≤E≤303 GeV (161 Events)
Experiment
Chew-Pignotti Model
Wang Model I
Wang Model II
NUMBER OF EVENTS
CHARGED TRACKS
10
20
30
40
50
60
70
2
4
6
8
10
12
14
16
18
20

FIGURE 9. Multiplicity distribution of charged particles in the final state for hydrogen events in the energy bin 303-437 GeV.

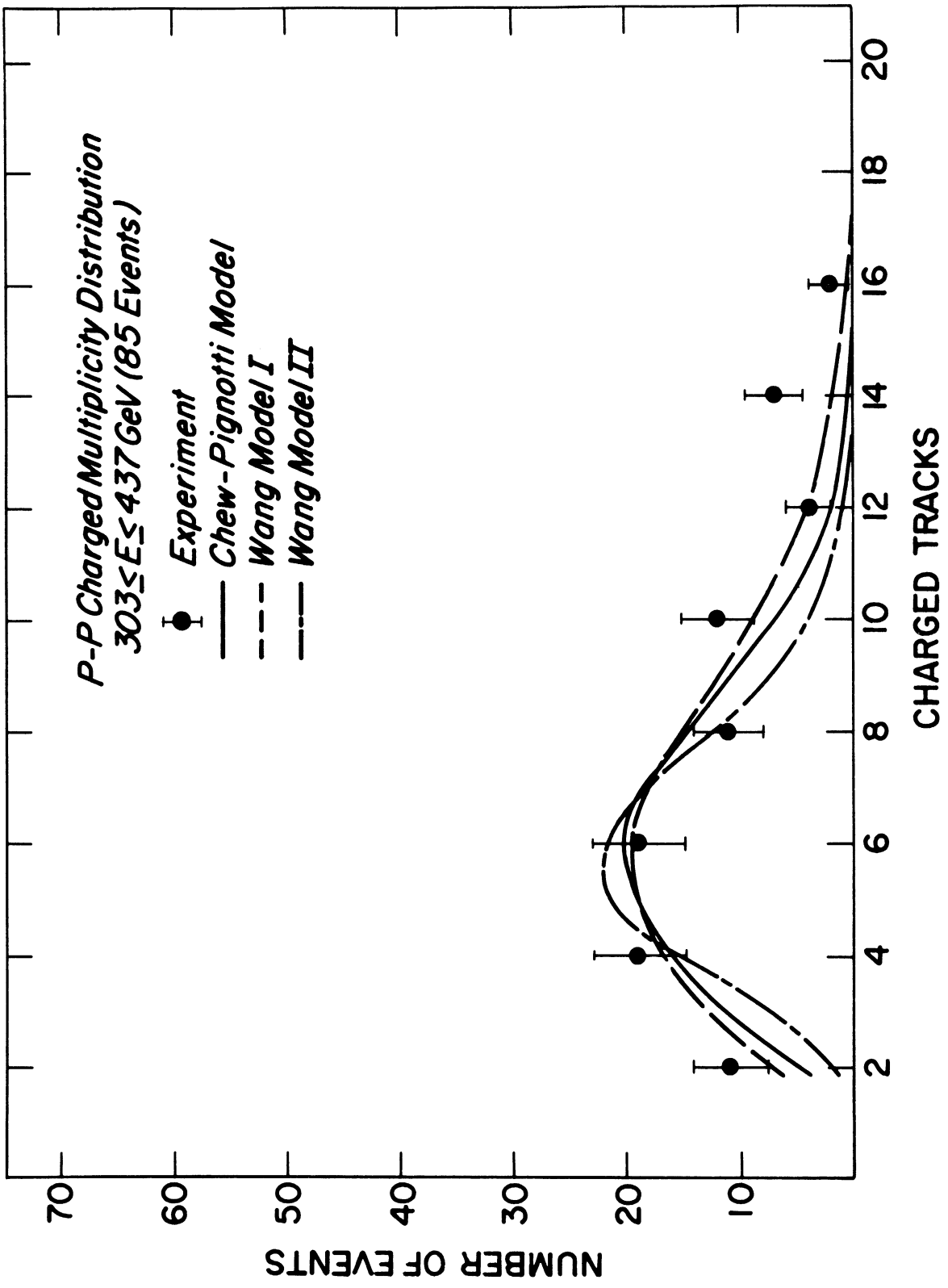
P-P Charged Multiplicity Distribution
303≤E≤437 GeV (85 Events)
Experiment
Chew-Pignotti Model
Wang Model I
Wang Model II
NUMBER OF EVENTS
CHARGED TRACKS
10
20
30
40
50
60
70
2
4
6
8
10
12
14
16
18
20

TABLE IV-4

Results of fitting the multiplicity distributions of charged parties in the final state from hydrogen to the multiperipheral model of Chew and Pignotti and the models of C. P. Wang.

Multiperipheral Model of Chew and Pignotti

En. Bin (GeV)	Average En. (GeV)	No. of Events (Expt.)	K (fitted)	$\langle n_\pi \rangle = g_m^2 X_o$ (fitted)	$\langle n_c \rangle = \frac{2}{3}\langle n_\pi \rangle + 2$	$\langle n_c \rangle$ (Expt.)
71-146	98.5	150	115.6	6.74	6.54	5.91
146-211	174.9	239	198.1	7.13	6.74	6.36
211-303	250.5	161	128.3	8.17	7.44	6.76
303-437	365.0	85	66.1	7.51	7.00	7.04

Models of C. P. Wang

En. Bin (GeV)	Average En. (GeV)	No. of Events (Expt.)	Model	K (fitted)	$\langle n_c \rangle$ (fitted)	$\langle n_c \rangle$ (Expt.)
71-146	98.5	150	I	128.3	5.96	5.91
			II	197.3	5.76	
146-211	174.9	239	I	218.4	6.24	6.36
			II	343.9	6.06	
211-303	250.5	161	I	142.3	6.92	6.76
			II	220.8	6.72	
303-437	365.0	85	I	73.9	6.62	7.04
			II	113.4	6.15	

pions. Wang model II, which predicts a Poisson distribution in simply the number of produced charged particles, is unable to describe the data. The prediction of the multiperipheral model, although providing a better fit than Wang model II, is observed to be inadequate in describing the data at the higher numbers of charged tracks. It seems that the most plausable explanation for this is that the allowed final states, as described by the coefficients in equation (I. 2), are not sufficient and that the possibility of production of particles other than just pions should be incorporated. In Wang model I, the possibility of production of charged particles other than pions is essentially included, since the arguments regarding charge conservation in terms of the production of $\pi^{\pm}$ pairs from "cells" within the interaction volume need not be restricted to only pions.

For the sake of completeness, the most statistically significant energy bin for carbon is shown in Fig. 10. In order to facilitate fitting the models, the multiplicity of odd pronged events was increased by one.

In concluding this section some comments should be made regarding the presence of pions in the cosmic ray hadron flux. As pointed out in Chapter I, approximately 30% of the interactions observed were due to charged pions. The models of Wang are insensitive to whether the initial state was pp or $\pi^{\pm}$ p. This was

FIGURE 10. Multiplicity distribution of charged particles in the final state for carbon events in the energy bin 146-211 GeV.

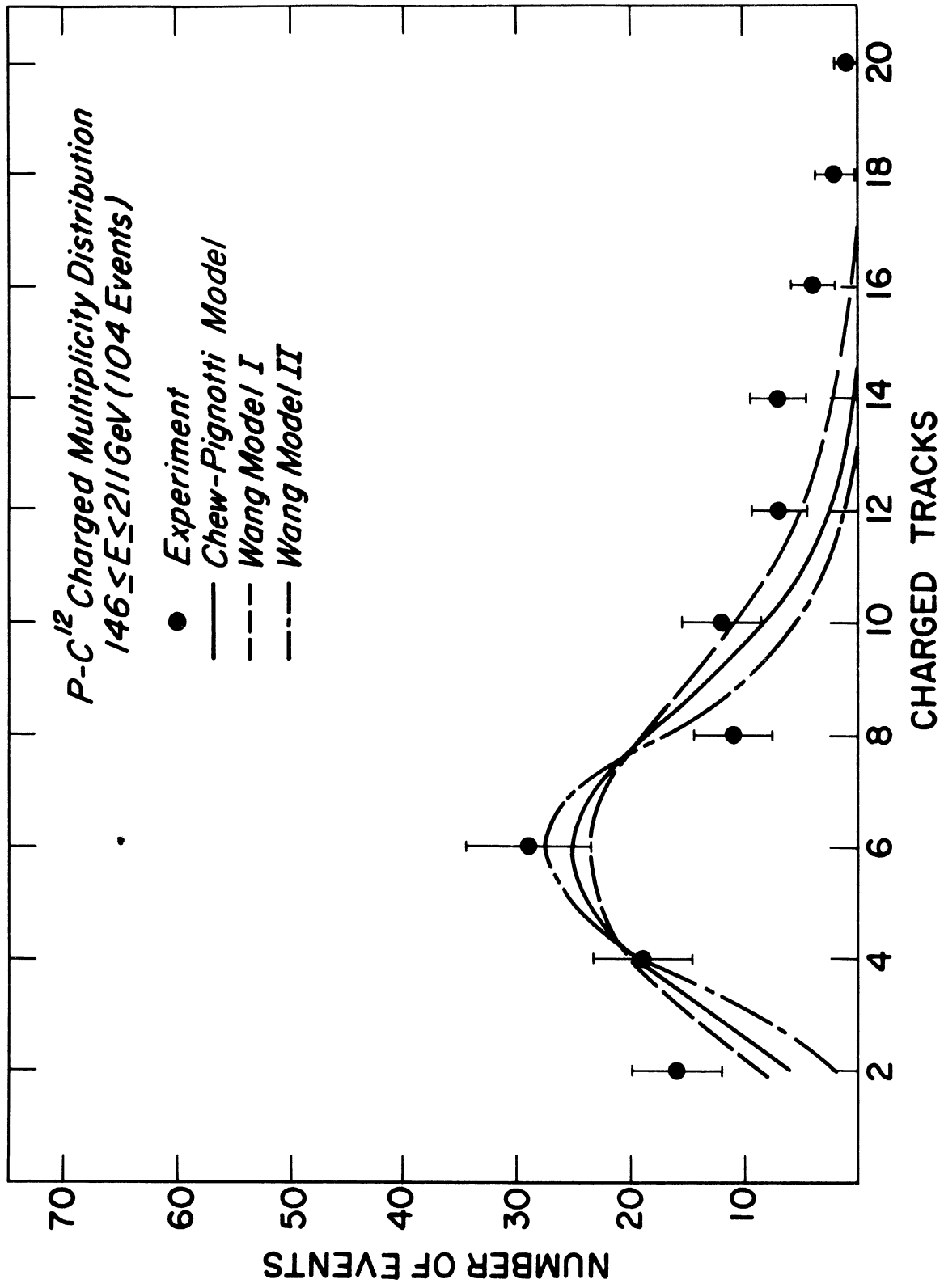
P-C12 Charged Multiplicity Distribution
146≤E≤211GeV (1104 Events)
Experiment
Chew-Pignotti Model
Wang Model I
Wang Model II
NUMBER OF EVENTS
CHARGED TRACKS
10
20
30
40
50
60
70
2
4
6
8
10
12
14
16
18
20

established by Wang[12] in fitting accelerator data from several experiments. Examination of the Wang distributions, as specified by equations (I. 4) and (I. 5), indicates that the only dependence on the initial state particles involves their charge. The prediction of the multiperipheral model, as specified by equations (I. 1) and (I. 2), contains a dependence on the rest mass of the incoming particle. This dependence enters via X_o. In addition, as discussed in Chapter I, the square of the coupling constant, g_m^2, has been found to be different for π^- p collisions than for pp collisions. J. W. Elbert, et. al.[11], however, have found that the functional form of equation (I. 2) is identical for π^- p and pp initial states. In terms of the multiperipheral model, the experimental distribution would, to a first approximation, be the sum of two distributions, one for the $\pi^{\pm}$ p events and the other for the pp events. Each of these distributions would have the same functional form, but would be Poisson in nature about a different mean value, given by the product of the corresponding g_m^2 and X_o. It was felt that the best way of fitting the multiperipheral model to the experimental distributions, in view of the above, was to allow the fit to determine the product, $g_m^2 X_o$.

B. Average Charged Multiplicity

The average multiplicity of charged particles in the final state, $\langle n_c \rangle$, for the five energy bins of interest were calculated

respectively for carbon and hydrogen directly from Tables IV-2 and IV-3 using

$$\langle n_c \rangle = \frac{\sum_{i=2}^{i_{max}} i\, n_i}{N_T}$$

where n_i is the number of events having i charged tracks in the final state and N_T is the total number of events in the energy bin of interest.

The values of the average multiplicity, as calculated above, were corrected for three effects listed below.

1. Delta ray production by charged final state particles.
2. Direct pair production by γ-rays originating from the decay of produced π^o's.
3. Unobservable tracks, due to produced particles not getting into the lower wide-gap spark chamber or particles whose tracks could not be resolved.

The first of these corrections has been discussed previously in Chapter III. The second and third of these were estimated in terms of the Monte Carlo program.[25] In addition, a calculation of the inelastic cross section from the data on hydrogen produced a value of about 19 mb for the pp cross section, after a correction for the π contamination was applied. This value is low compared to the value of 29.7 mb found by Chew and Pignotti[10] in fitting pp data

from 12.88 to 28.44 GeV/c. The low value of the cross section is understood in terms of a systematic underestimate of the energy of interacting events as compared to that of non-interacting events, as determined by the calorimeter. The energy underestimate can be accounted for in terms of the Monte Carlo program and shown to be essentially independent of energy. It is also of interest to note that the energy estimate from the angular distribution of charged secondaries is larger than that provided by the calorimeter. Based on these results regarding the cross section, the average energy of each bin, as determined by the calorimeter, was increased to a value required to renormalize the cross section to 29 mb. The results of corrections made to $\langle n_c \rangle$ are summarized in Table IV-5. The errors assigned to $\langle n_c \rangle$, as given in Table IV-5, were calculated from

$$\pm \sqrt{\frac{\langle n_c^2 \rangle - \langle n_c \rangle^2}{N_T}} \quad .$$

It should be noted at this time that all model fitting and plotting was done in terms of the corrected values of $\langle n_c \rangle$, as given in the righthand column of Table IV-5. The energy values used were those required to normalize σ_{pp} to 29 mb.

Shown in Fig. 11 is a comparison of the average charged multiplicities as determined for hydrogen and carbon. It is

TABLE IV-5

Summary of corrections made to the data on average charged multiplicity

En. Bin (GeV)	Average En. calorimeter (GeV)	$\langle n_c \rangle$ uncorrected	Error in $\langle n_c \rangle$	$\langle n_c \rangle$ corrected for δ-rays produced by secondaries	(Average En.)/.86 to give σ_{pp} = 29 mb (GeV)	$\langle n_c \rangle$ corrected for γ-ray conversion and missing tracks (based on Monte Carlo)
			Hydrogen			correction term = -.40
71-146	98.5	5.91	± .27	5.82	114.5	5.42
146-211	174.9	6.36	± .22	6.27	203.4	5.87
211-303	250.5	6.76	± .30	6.66	290.7	6.26
303-437	365.0	7.04	± .40	6.94	424.4	6.54
437-905	588.2	7.56	± .61	7.45	684.0	7.05
			Carbon			correction term = -.49
71-146	95.7	7.00	± .44	6.88	111.3	6.39
146-211	177.1	7.07	± .42	6.94	205.9	6.45
211-303	247.2	7.80	± .58	7.66	287.4	7.17
303-437	344.1	8.21	±1.26	8.06	400.1	7.57
437-905	564.2	9.41	±1.07	9.24	656.0	8.75

FIGURE 11. The average charged multiplicity in hydrogen and carbon plotted as a function of the laboratory energy of the incident hadron.

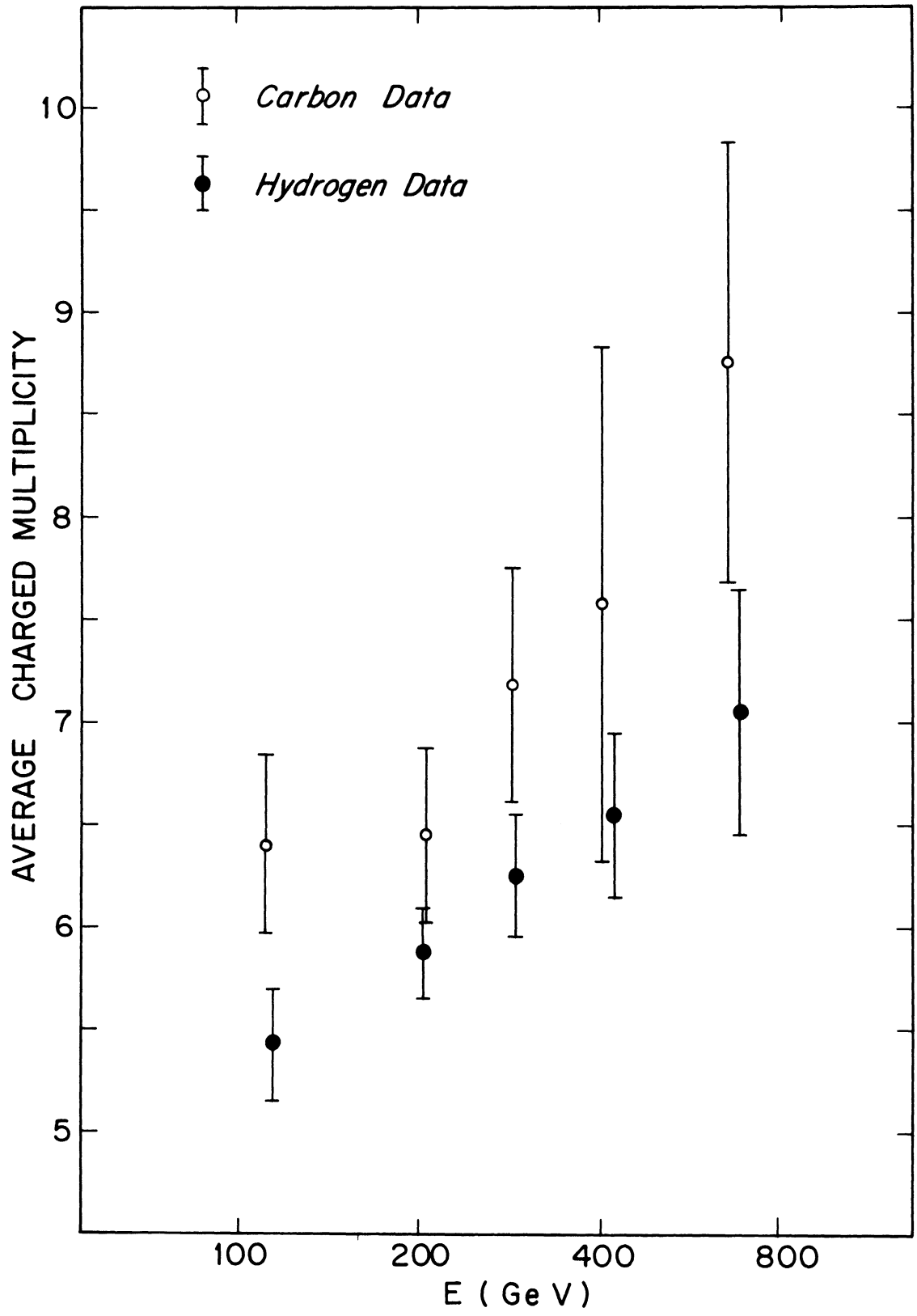
Carbon Data
Hydrogen Data
AVERAGE CHARGED MULTIPLICITY
10
9
8
7
6
5
100
200
400
800
E (Ge V)

observed that over the range of energies considered

$$\langle n_c \rangle \text{ carbon} - \langle n_c \rangle \text{ hydrogen} \cong 1 \quad .$$

A possible explanation for the larger value of $\langle n_c \rangle$ observed in carbon might be made in terms of additional secondary interactions with other nucleons in the carbon nucleus.

The hydrogen data has been fitted to the predictions of three models, as indicated in Fig. 12. Data points on average charged muliplicities for pp collisions from two accelerator experiments, as taken from Barashenkov, et. al. [3], have been included in Figs. 13 and 14. In Fig. 13 the accelerator points have been included in the fit, while for Fig. 14 the functions were fitted to our data alone and merely extrapolated to the accelerator energies. For each model a χ^2 fit in terms of the available parameters was made to the experimental data. A summary of the parameter values obtained in fitting each model to our data alone, and to our data plus the accelerator data is presented in Table IV-6. The success of the $\ell n E$ dependence, as predicted by the multiperipheral model, over the entire range of energy as shown in Fig. 13 is quite striking. It can be concluded that there is a definite preference for a $\ell n E$ dependence over the $E^{\frac{1}{4}}$ dependence of the hydrodynamical model. The isobar-pionization model, which predicts an energy dependence of the form $A + B\, E^{\frac{1}{2}}$, is observed to fit very well

FIGURE 12. The hydrogen data on average charged multiplicity as compared to the predictions of the multiperipheral model of Chew and Pignotti, the hydrodynamical model of Belenjki and Landau and the isobar-pionization model of Pal and Peters.

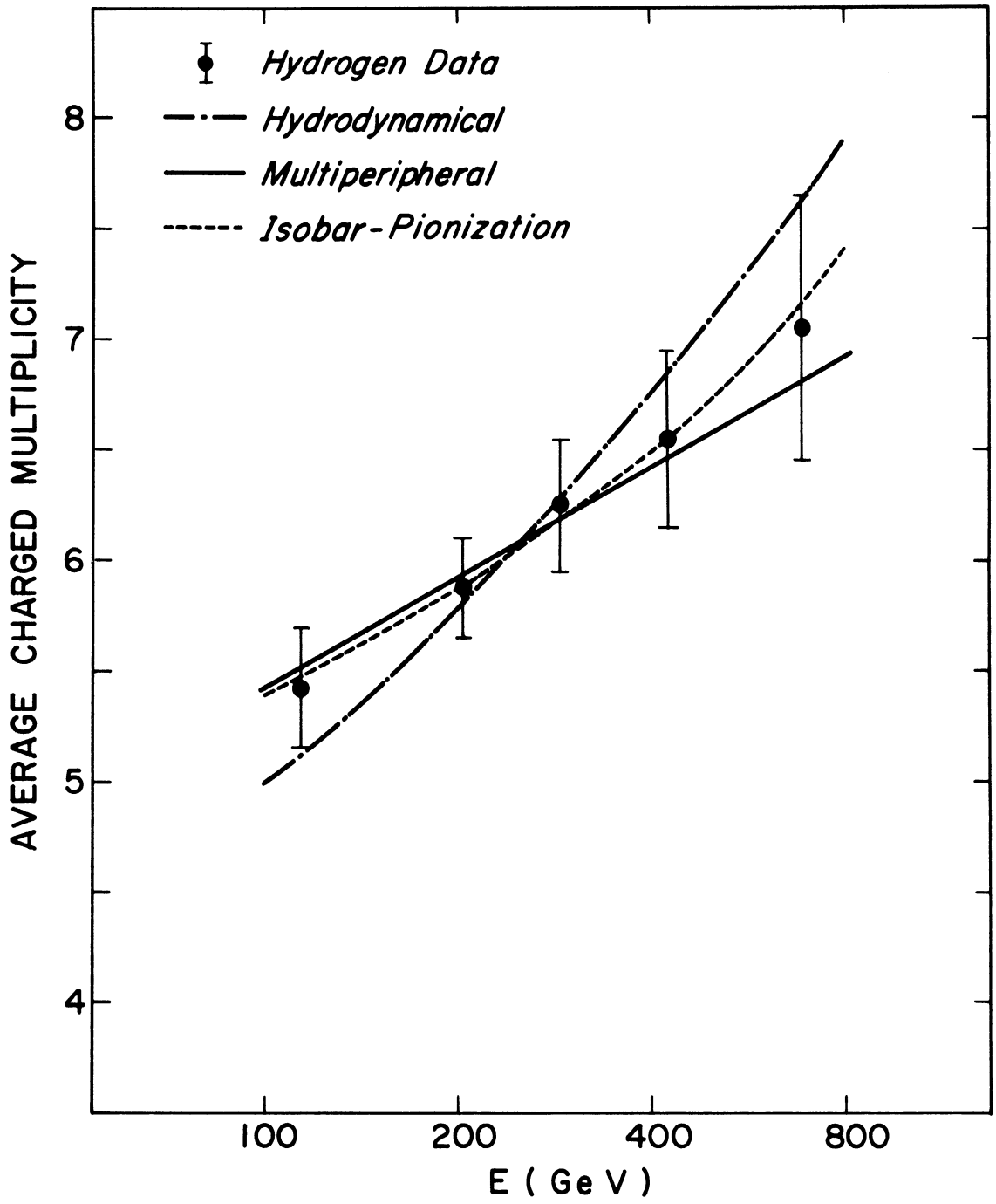
Hydrogen Data
Hydrodynamical
Multiperipheral
Isobar-Pionization
AVERAGE CHARGED MULTIPLICITY
8
7
6
5
4
100
200
400
800
E (Ge V)

FIGURE 13. Comparison of the average charged multiplicity in hydrogen, including two data points from accelerator experiments, to the multiperipheral model of Chew and Pignotti, the hydrodynamical model of Belenjki and Landau and the isobar-pionization model of Pal and Peters.

The accelerator data points are taken from reference 3.

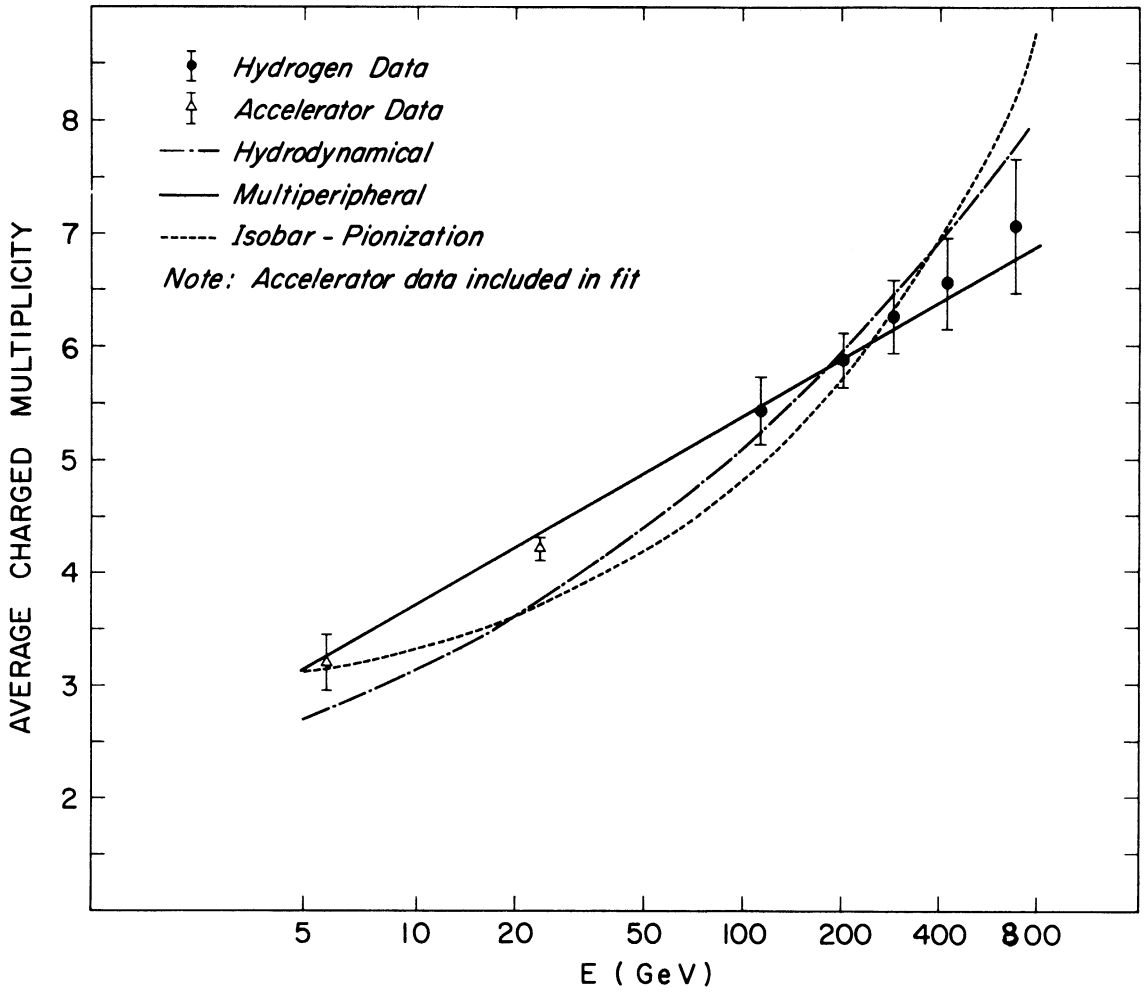
Hydrogen Data
Accelerator Data
Hydrodynamical
Multiperipheral
Isobar - Pionization
Note: Accelerator data included in fit
AVERAGE CHARGED MULTIPLICITY
2
3
4
5
6
7
8
5
10
20
50
100
200
400
800
E (GeV)

FIGURE 14. Comparison of the average charged multiplicity in hydrogen from this experiment only, but where the fitted functions have been extrapolated to accelerator energies, to the multiperipheral model of Chew and Pignotti, the hydrodynamical model of Belenjki and Landau and the isobar-pionization model of Pal and Peters.

The accelerator data points are taken from reference 3.

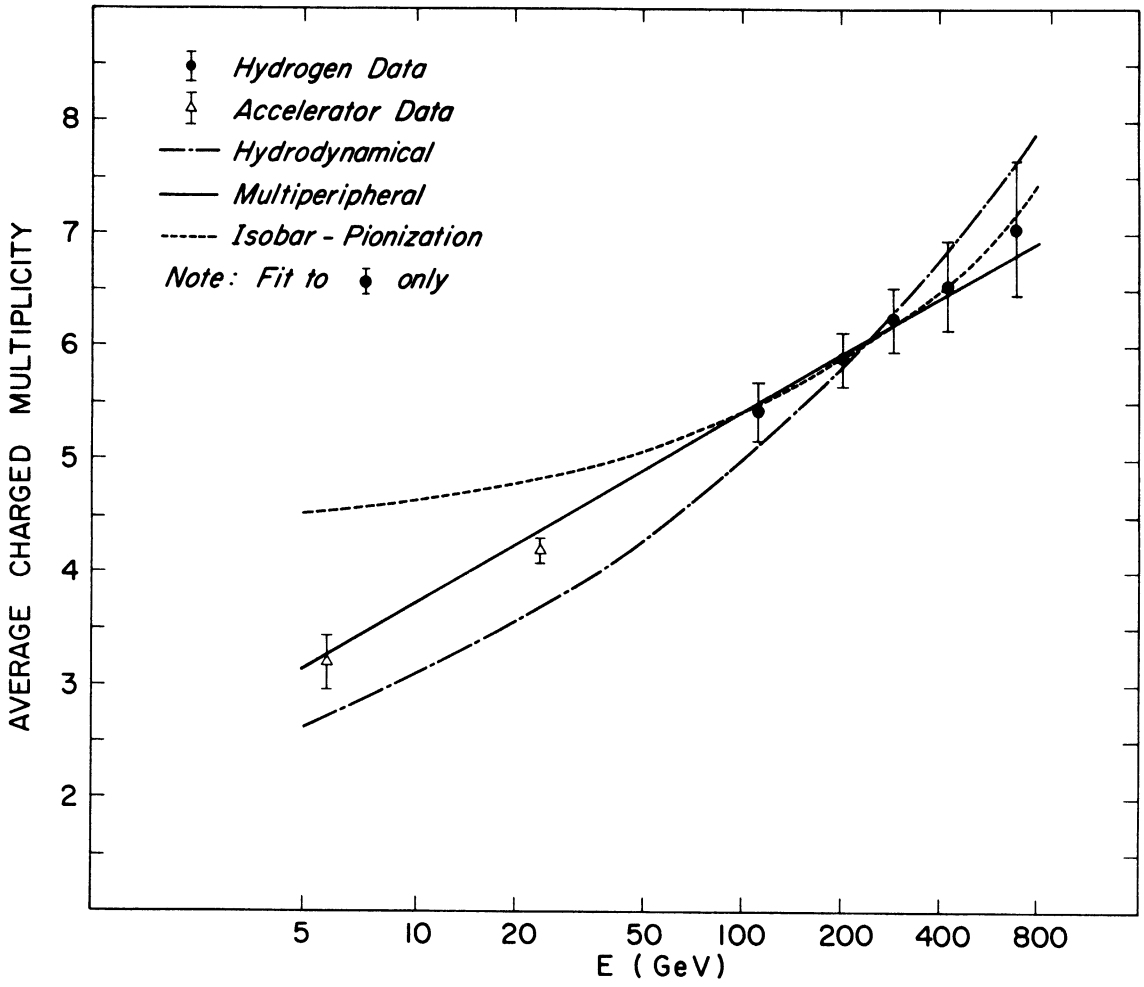
Hydrogen Data
Accelerator Data
Hydrodynamical
Multiperipheral
Isobar - Pionization
Note: Fit to ● only
AVERAGE CHARGED MULTIPLICITY
2
3
4
5
6
7
8
5
10
20
50
100
200
400
800
E (GeV)

TABLE IV-6

Summary of the results of fitting the hydrogen data on average charged multiplicity to the multiperipheral model of Chew and Pignotti, the hydrodynamical model of Belenjki and Landau and the isobar-pionization model of Pal and Peters.

Model	Function fitted	Values of Fitted Parameters	
		Our data only	Our data + 2 accel. points
Hydrodynamical	$\frac{2}{3}(AE^{\frac{1}{4}} + 1)$	A = 2.04	A = 2.09
Multiperipheral	$\frac{2}{3}(G \ln {}^{E}/_{m}) + 2$	G = 1.10	G = 1.08
Isobar - Pionization	$\frac{2}{3}(A + B\, E^{\frac{1}{2}}) + 2$	A = 3.42 B = .17	A = .97 B = .32

to our data taken by itself, but does not fit well over the broader energy region including the accelerator data.

C. Angular Distributions

The angular distributions of the charged particles in the final state have been studied in terms of a modified Duller-Walker formulation, as described in Chapter I. At this point it should be recalled that the angles of the charged secondaries relative to the beam direction were specified in a projected laboratory system. This was necessary because the events were photographed in 90^{o} stereo and no attempt was made to correlate the tracks of the secondaries from the two views. The two views corresponded to two independent projected systems.

For each energy bin of interest an "integrated event" was formed consisting of the tracks from all events having 3 or more charged tracks in the final state; the two views being summed together. The angle of each track, θ_p, relative to the beam direction was known in the projected system so that angular distributions of these "integrated events" could be studied.

Presented in Figs. 15 and 16 are the number distributions of charged tracks in $\log_{10}\tan\theta_p$ coordinates for the energy bins 146-211 and 211-303 GeV. Shown in Figs. 17 and 18 are the corresponding modified Duller-Walker plots. The modified Duller-Walker plots clearly show a two-branch structure

FIGURE 15. $\text{Log}_{10} \tan\theta_p$ distribution of the charged particles in the final state for hydrogen events of multiplicity $\geq$ 3 in the energy bin 146-211 GeV.

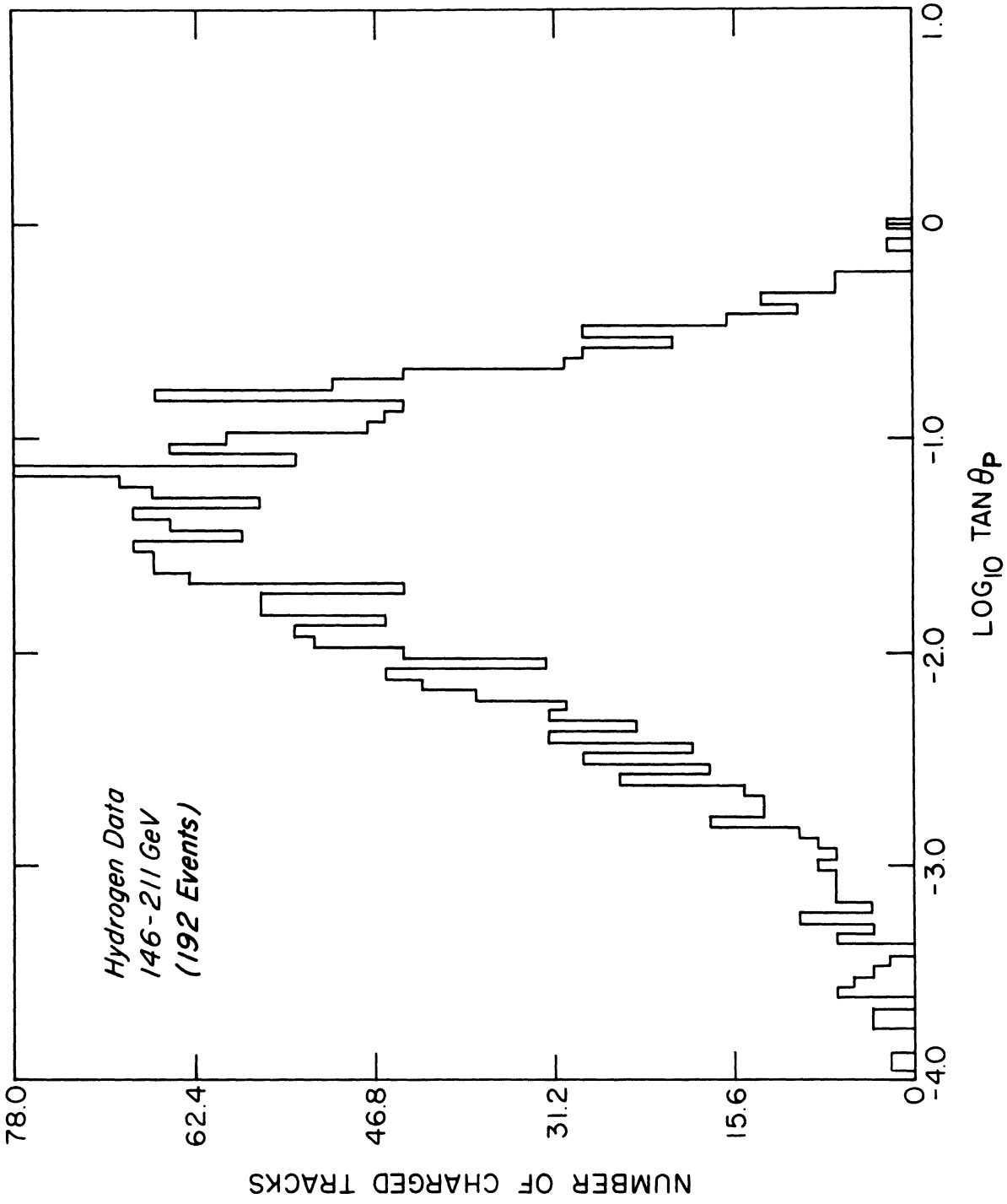
Hydrogen Data
146-211 GeV
(192 Events)
NUMBER OF CHARGED TRACKS
78.0
62.4
46.8
31.2
15.6
0
1.0
0
-1.0
-2.0
-3.0
-4.0
LOG10 TAN θP

FIGURE 16. $\text{Log}_{10} \tan\theta_p$ distribution of the charged particles in the final state for hydrogen events of multiplicity $\geq$ 3 in the energy bin 211-303 GeV.

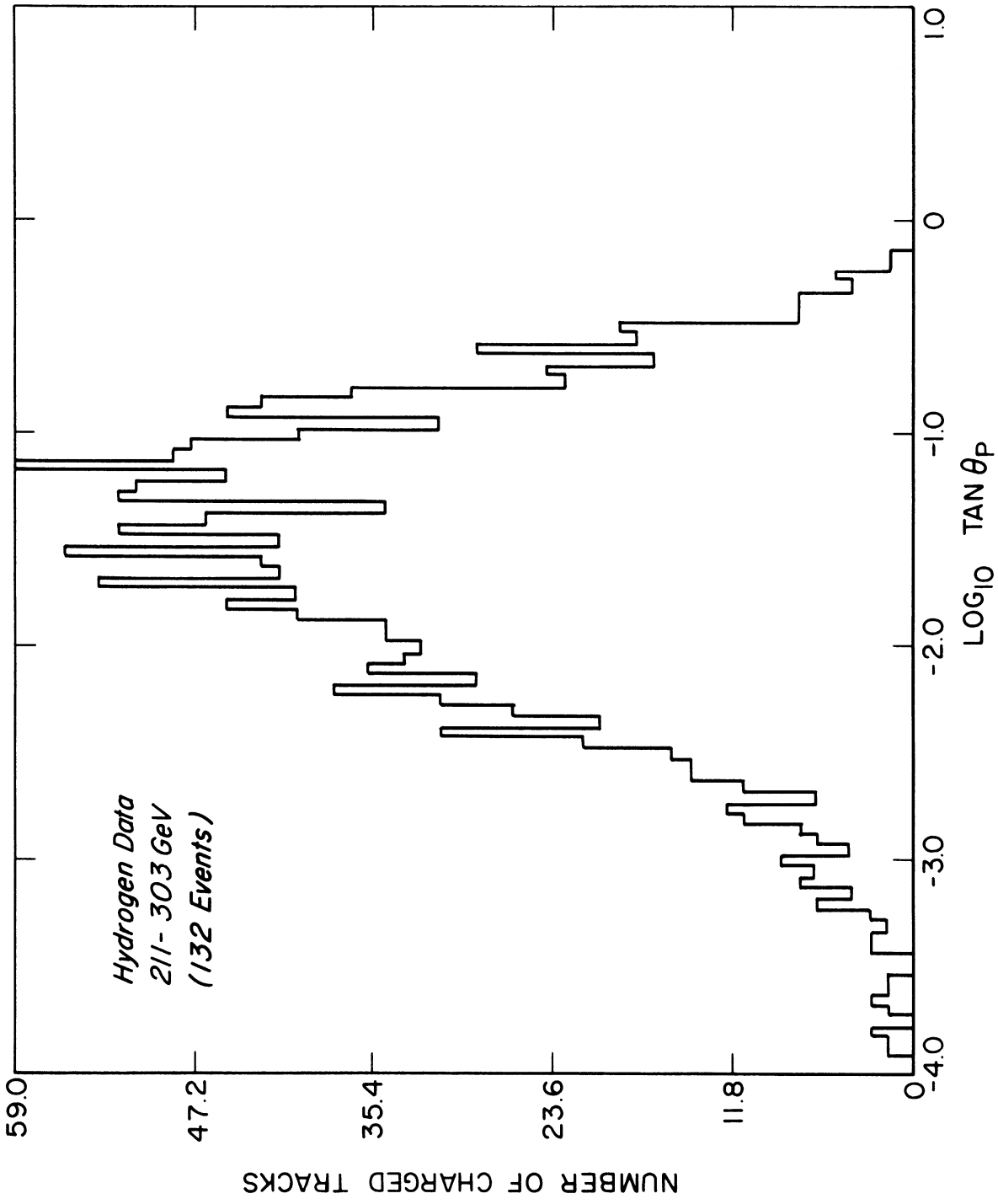
Hydrogen Data
2/1- 303 GeV
(132 Events)
NUMBER OF CHARGED TRACKS
59.0
47.2
35.4
23.6
11.8
0
-4.0
-3.0
-2.0
-1.0
0
1.0
LOG10 TAN θP

FIGURE 17. Modified Duller-Walker plot for the charged particles in the final state for hydrogen events of multiplicity $\geq$ 3 in the energy bin 146-211 GeV as compared to the C. M. angular distributions indicated.

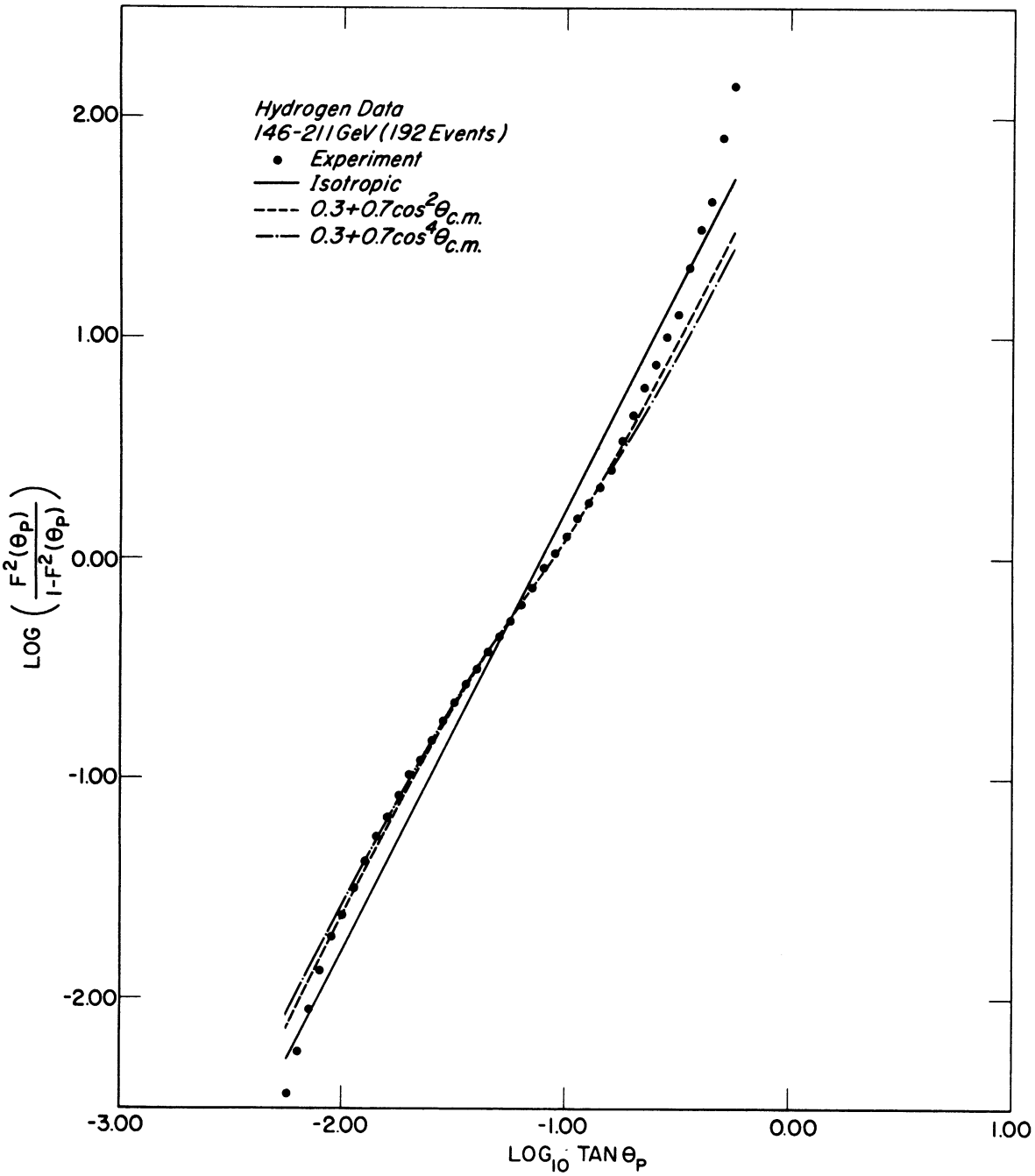
Hydrogen Data
146-211 GeV (192 Events)
Experiment
Isotropic
0.3+0.7cos²θc.m.
0.3+0.7cos⁴θc.m.
2.00
1.00
0.00
-1.00
-2.00
-3.00
-2.00
-1.00
0.00
1.00
LOG (F²(θP) / 1-F²(θP))
LOG10 TAN θP

FIGURE 18. Modified Duller-Walker plot for the charged particles in the final state for hydrogen events of multiplicity $\geq$ 3 in the energy bin 211-303 GeV as compared to the C. M. angular distributions indicated.

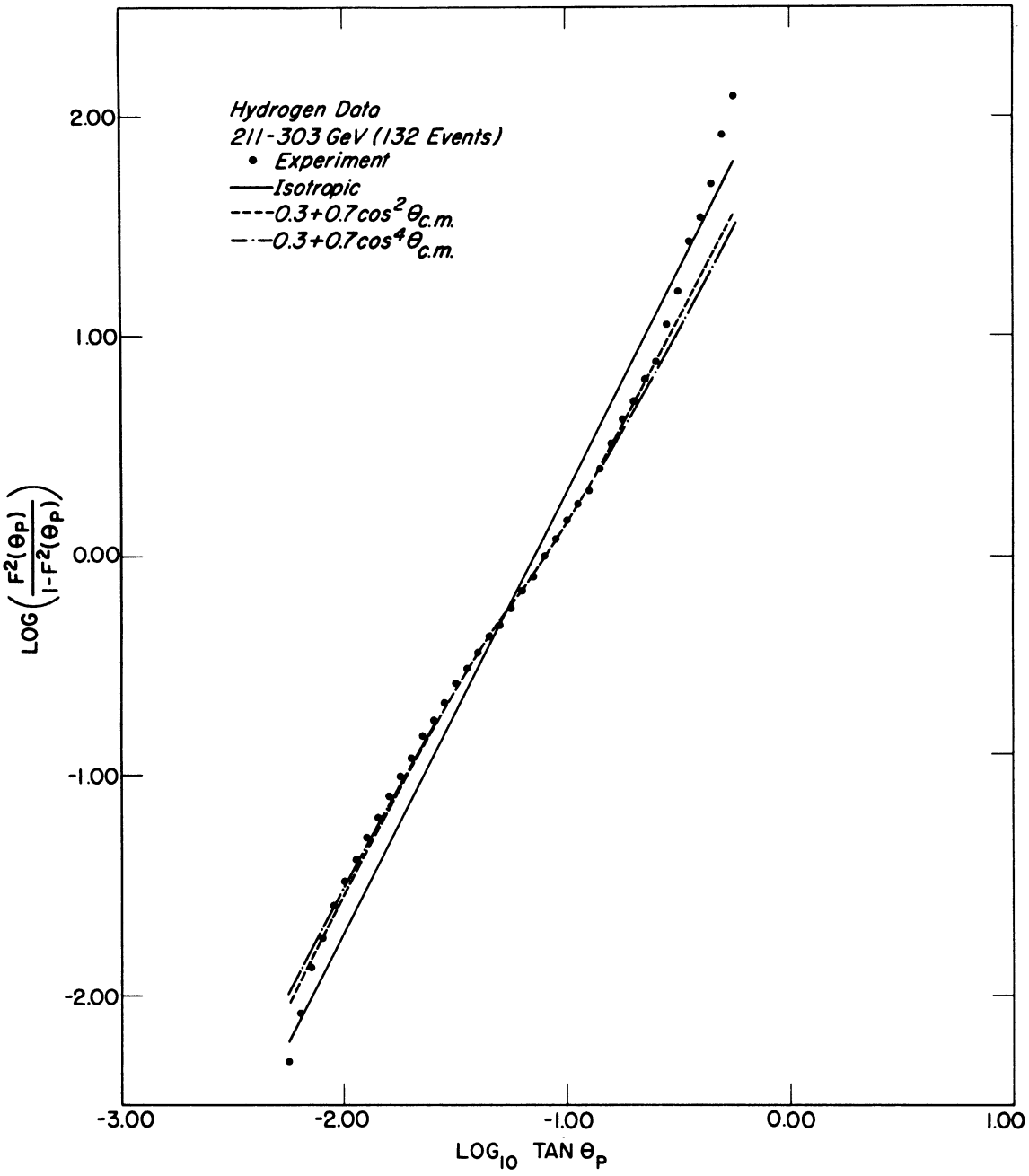
Hydrogen Data
211-303 GeV (132 Events)
• Experiment
——Isotropic
----0.3+0.7cos² θc.m.
—·—0.3+0.7cos⁴ θc.m.
2.00
1.00
0.00
-1.00
-2.00
-3.00
-2.00
-1.00
0.00
1.00
LOG (F²(θP) / 1-F²(θP))
LOG10 TAN θP

corresponding to a non-isotropic C. M. angular distribution. Also shown in Figs. 17 and 18 are the best fits to a C. M. isotropic distribution and to C. M. distributions of the form $A + B \cos^{M}\theta_{c.m.}$ $(A + B = 1,\ M = 2, 4)$. A χ^2 fit to the experimental data was made in terms of the two parameters B and γ, as described in Chapter I. Because of a certain amount of poisoning in the extreme forward and backward directions, the fit was constrained to fit only the data points falling between -1.00 and 0.05 on the $\text{Log}\left(\frac{F^2(\theta_p)}{1-F^2(\theta_p)}\right)$ scale. In making the Duller-Walker plots a correction was applied for the unobserved recoil proton in about half of the events. This was necessary to maintain symmetry in the C. M. system between the incident and target proton. It is observed that over the region of data fitted, a C. M. distribution of the form $0.3 + 0.7 \cos^{M}\theta_{c.m.}$ (M = 2 or 4) describes the data well. The fit is relatively insensitive to the power of $\cos\theta_{c.m.}$, so that in this work the value of M cannot be specified, except that it is at least as large as 2. The degree of anisotropy, B, however, seems to be fairly well specified at a value of 0.7 for the energy bins shown.

A summary of the fitted parameters, B and γ, is presented in Tables IV-7 and IV-8 for hydrogen and carbon respectively. These tables indicate that in general the energy determined by fitting the angular distributions is larger than determined by the

TABLE IV-7

Summary of Angular Distribution Fits (Hydrogen)

En. Bin	Average En. (Expt.)	γ (Expt.)	γ (Fitted)	En. (fitted)	B (fitted)	M
71-102	85.3	6.78	9.93	184.0	--	0
			10.03	187.8	0.54	2
			10.05	188.5	0.56	4
102-146	121.0	8.06	11.58	250.6	--	0
			11.82	261.2	0.56	2
			11.83	261.6	0.56	4
146-211	174.9	9.68	12.87	309.8	--	0
			13.00	316.1	0.66	2
			13.13	322.5	0.67	4
211-303	250.5	11.58	14.02	367.8	--	0
			14.20	377.3	0.66	2
			14.31	383.2	0.67	4
303-437	365.0	13.97	13.13	322.5	--	0
			12.92	312.2	0.72	2
			13.04	318.1	0.72	4
437-629	517.8	16.63	14.07	370.4	--	0
			14.50	393.5	0.70	2
			14.60	398.9	0.69	4

TABLE IV-8

Summary of Angular Distribution Fits (Carbon)

En. Bin	Average En. (Expt.)	γ (Expt.)	γ (Fitted)	En. (fitted)	B (fitted)	M
146-211	177.1	9.74	11.11	230.6	--	0
			11.27	237.3	.68	2
			11.38	243.0	.68	4
211-303	247.2	11.50	12.71	302.1	--	0
			13.03	317.6	.70	2
			13.17	324.5	.70	4
303-437	344.1	13.56	12.16	276.5	--	0
			12.06	271.9	.64	2
			12.13	275.1	.66	4

calorimeter. Also, there does not seem to be any significant energy dependence on B over the range of energy considered.

D. Inelasticity

The average inelasticity of the events in each energy bin was estimated in terms of the 2-center model of Cocconi[19], for both the hydrogen and carbon data. The method consists of fitting the forward and backward branches of the modified Duller-Walker plots separately to determine γ_{b_1} and γ_{b_2}. The quantities γ_{b_1} and γ_{b_2}, along with the other quantities of interest, have been defined in Chapter I. Presented in Table IV-9 are the results of this fitting procedure. It is seen that the energies, as estimated by this approach, are consistent with those found in the previous section. The estimated inelasticity is observed to be independent of energy for both hydrogen and carbon with the value for carbon being larger than for hydrogen.

E. Summary of Conclusions

A summary has been provided below of the conclusions drawn from the study, described in this paper, regarding the interactions of charged cosmic ray hadrons with hydrogen and carbon targets over an energy range of 70-600 GeV.

1. The hydrogen data on multiplicity distributions of charged particles in the final state is best described by a Poisson

TABLE IV-9

Summary of 2 - Center Model Fits to Estimate the Inelasticity

En. Bin	Average En. (Expt.)	γ_{b_1}	γ_{b_2}	γ (Theory)	En (Theory)	γ_f	γ_N	ρ
			Hydrogen					
71-102	85.3	31.50	3.51	10.52	206.7	1.50	5.81	.45
102-146	121.0	33.02	4.03	11.54	249.1	1.43	7.21	.38
146-211	174.9	40.97	3.90	12.65	299.2	1.62	7.54	.40
211-303	250.5	43.31	3.88	12.97	314.5	1.67	6.93	.47
303-437	365.0	41.02	3.95	12.73	303.0	1.61	6.89	.46
437-629	517.8	42.53	4.47	13.79	355.8	1.54	8.09	.41
			Carbon					
71-102	83.6	36.34	3.86	11.85	262.5	1.53	5.83	.51
102-146	120.9	34.74	3.53	11.08	229.4	1.57	2.76	.75
146-211	177.1	42.10	3.48	12.10	273.8	1.74	4.29	.65
211-303	247.2	38.84	3.65	11.91	265.0	1.63	3.85	.68
303-437	344.1	40.66	4.31	13.24	327.8	1.54	3.73	.72
437-629	498.7	38.64	4.33	12.94	313.3	1.49	3.66	.72

distribution in the mean number of pairs of produced charged particles.

2. The hydrogen data on the average multiplicity of charged particles in the final state definitely favors an energy dependence of ℓnE (multiperipheral model) as opposed to a dependence of $E^{\frac{1}{4}}$ (hydrodynamical model).

3. The average charged multiplicity in carbon is larger than in hydrogen. The difference, averaged over the range of energy, being about 1.0.

4. The C. M. angular distributions of charged particles in the final state are non-isotropic and can be described by a C. M. distribution of the form $0.3 + 0.7 \cos^{M}\theta_{c.m.}$ where M is at least as large as 2.

5. The inelasticity is independent of energy for both target materials with the value for carbon being larger than for hydrogen.

BIBLIOGRAPHY

1. Jarlskog, G., "A Survey of Multiple Particle Production in Nucleon-Nucleon Collisions From Cosmic Ray Physics" Lund Electron Synchrotron (LUSY), paper 6809, presented at a seminar held in Lund, Sweden,(1968).

2. Yamada, S. and M. Koshiba, "Phys. Rev." 157, No. 5, 1279, (1967).

3. Barashenkov, V. S., et. al., "Fortschritte der Physik" 14, 357, (1966).

4. Lohrmann, E., M. W. Teucher, and Marcel Schein, "Phys. Rev." 122, No. 2, 672, (1961).

5. Castagnoli, C., et. al., "Nuovo Cimento," 10, 1539, (1953).

6. Duller, N. M., and W. D. Walker, "Phys. Rev." 93, No. 1, 215, (1954).

7. Dobrotin, N. A., et. al., "Canadian Journal of Physics" 46, S675, (1968).

8. Eremenko, Yu. A., et. al., "Canadian Journal of Physics" 46, S697, (1968).

9. Jones, L. W., "Proposal to Study Nucleon-Nucleon Total Cross Sections in the Energy Range from 50 to 1000 GeV using Cosmic Rays" University of Michigan Proposal ORA-67-724-F1, (January, 1967) (unpublished).

10. Chew, G. F., and A. Pignotti, "Phys. Rev." 176, No. 5, 2112, (1968).

11. Elbert, J. W., A. R. Erwin, W. D. Walker and J. W. Walters, "A Comparison of Models for Neutral and Charged Pion Multiplicities Observed in 25 GeV/c π^-p Collisions", University of Wisconsin preprint, (1969) (to be published in "Nuclear Physics").

12. Wang, C. P., "Phys. Rev." 180, No. 5, 1463, (1969).

13. Belen'kji, S. Z., and L. D. Landau, "Nuovo Cimento Suppl.", 3, 15, (1956).

14. Fermi, E., "Prog. Theor. Phys.", 5, 570, (1950) and "Phys. Rev.", 81, No. 5, 683, (1951).

15. Pal, Y., and B. Peters, "Mat. Fys. Medd Dan Vid. Selsk" 33, No. 15, 3, (1964).

16. Ciok, P., et. al., "Nuovo Cimento", 10, 741, (1958).

17. Niu, K., "Nuovo Cimento", 10, 994, (1958).

18. Gierula, J., D. M. Haskin and E. Lohrmann, "Phys. Rev.," 122, No. 2, 626, (1961).

19. Cocconi, G., "Phys. Rev.," 111, No. 6, 1699, (1968).

20. Grigorov, N. W., et. al., "Soviet Physics JETP", 7, 348, (1958).

21. Murzin, V. S., Progress in Elementary Particles and Cosmic Ray Physics, 9 North Holland Publishing Co., Amsterdam, (1967).

22. Lyon, D. E., and A. Subramanian, "Design of Ionization Spectrometers using Iron and Scintillators for the Detection of Hadrons in the 100-1000 BeV Range," MURA preprint, 725, (1967) (unpublished).

23. Pinkau, K., and K. V. Thompson, "Rev. Sci. Instr.," 37, 302, (1966).

24. Jones, W. V., "Phys. Rev.," 187, No. 5, 1868, (1969).

25. Lyon, D. E., Private Communication, University of Michigan, Ann Arbor, Michigan.

26. Ritson, D. M., Techniques of High Energy Physics, Interscience Publishers, Inc., N. Y. (1961).

27. Bieriens, D. D., Nouvelles Tables D' Integrales Definies, G. E. Stechert, Inc., N. Y. (1939).

APPENDIX

Duller-Walker Formulation in a Projected System

The Duller-Walker[6] approach to a study of angular distributions of secondaries produced in strong interactions has been reformulated in terms of a projected laboratory system. Presented here are the steps involved in this reformulation for center of mass system (C. M. S.) differential number density distributions of produced secondaries of the form

$$N(\theta_{c.m.}, \phi_{c.m.})d\Omega_{c.m.} = Kd\Omega_{c.m.} \qquad \text{(Isotropic)}$$

and

$$N(\theta_{c.m.}, \phi_{c.m.})d\Omega_{c.m.} = K(A + B\cos^{M}\theta_{c.m.})d\Omega_{c.m.} \quad \begin{matrix} M = 2, 4 \\ A + B = 1 \end{matrix}$$

where $\theta_{c.m.}$ and $\phi_{c.m.}$ are the zenith and azimuthal angles of a secondary with respect to the beam direction and $d\Omega_{c.m.}$ is the differential solid angle. In essence one successively transforms the distribution from the C. M. S. to the laboratory system (L.S.) and from the L. S. to the projected L. S., and then integrates the resulting distribution, properly normalized, between appropriate limits to obtain an expression for the fraction of secondaries falling within a projected cone, that is

$$N(\theta_{c.m.}, \phi_{c.m.})d\Omega_{c.m.} \rightarrow N(\theta_L, \phi_L)d\Omega_L \rightarrow N(\theta_X, \theta_Y)d\Omega_{X,Y}$$

with

$$F(\theta_p) = \frac{1}{N} \int_{-\theta_p}^{\theta_p} \int_{-\frac{\pi}{2}}^{\frac{\pi}{2}} N(\theta_X, \theta_Y)\, d\Omega_{X,Y}$$

where N is the total number of secondaries. The transformation equations which were used are summarized as follows

$$\tan \theta_L = \frac{1}{\gamma} \tan \frac{\theta_{c.m.}}{2} \qquad (A.1)$$

$$\phi_L = \phi_{c.m.} \qquad (A.2)$$

$$d\alpha_1 d\alpha_2 = \frac{\partial(\alpha_1, \alpha_2)}{\partial(\eta_1, \eta_2)}\, d\eta_1\, d\eta_2 \qquad (A.3)$$

$$\tan^2 \theta_L = \tan^2 \theta_X + \tan^2 \theta_Y \qquad (A.4)$$

$$\tan \phi_L = \frac{\tan \theta_Y}{\tan \theta_X} \qquad (A.5)$$

I. Solid Angle Transformations

The element of solid angle in the C. M. system is

$$d\Omega_{c.m.} = \sin \theta_{c.m.}\, d\theta_{c.m.}\, d\phi_{c.m.}$$

which using (A. 1) and (A. 3) transforms to

$$d\Omega_L = \frac{4\gamma^2 \tan\theta_L \sec^2\theta_L}{(1 + \gamma^2 \tan^2\theta_L)^2} d\theta_L d\phi_L$$

and further transforms to

$$d\Omega_{X,Y} = \frac{4\gamma^2 \sec^2\theta_X \sec^2\theta_Y}{[1 + \gamma^2(\tan^2\theta_X + \tan^2\theta_Y)]^2} d\theta_X d\theta_Y \qquad (A.6)$$

with the aid of equations (A. 3), (A. 4) and (A. 5).

II. Normalization

For the isotropic case, with N being the total number of secondaries, one has

$$N = K\int_o^{\pi}\int_o^{2\pi} \sin\theta_{c.m.} d\theta_{c.m.} d\phi_{c.m.}$$

or

$$K = \frac{N}{4\pi}$$

For the bi-model case one has

$$N = K\int_o^{\pi}\int_o^{2\pi} (A + B\cos^M\theta_{c.m.})\sin\theta_{c.m.} d\theta_{c.m.} d\phi_{c.m.}$$

or

$$K = \frac{N}{4\pi(A + \frac{B}{M+1})}$$

III. Projected Fraction-Isotropic Case

The projected fraction is

$$F(\theta_p) = \frac{1}{N} \int_{-\theta_p}^{\theta_p} \int_{-\frac{\pi}{2}}^{\frac{\pi}{2}} \frac{N}{4\pi} \, d\Omega_{X,Y}$$

which using (A. 6) becomes

$$F(\theta_p) = \frac{\gamma^2}{\pi} \int_{-\theta_p}^{\theta_p} \int_{-\frac{\pi}{2}}^{\frac{\pi}{2}} \frac{\sec^2 \theta_X \sec^2 \theta_Y}{[1 + \gamma^2(\tan^2 \theta_X + \tan^2 \theta_Y)]^2} d\theta_X d\theta_Y \, .$$

Integrating first with respect to θ_Y and then θ_X, noting in each case that the integrand is an even function of the variable of integration readily yields

$$F(\theta_p) = \frac{\gamma \tan \theta_p}{\sqrt{1 + \gamma^2 \tan^2 \theta_p}} \, .$$

This in turn can be rewritten as

$$\frac{F^2(\theta_p)}{1 - F^2(\theta_p)} = \gamma^2 \tan^2 \theta_p \qquad (A.7)$$

or

$$\log \frac{F^2(\theta_p)}{1 - F^2(\theta_p)} = 2 \log \tan \theta_p + 2 \log \gamma \qquad (A.8)$$

which is of the identical functional form as that found by Duller

and Walker relating the fraction in the L. S., except that in the projected system the fraction is squared.

IV. Projected Fraction - $A + B \cos^2 \theta_{c.m.}$ Case

Before writing down the integral for the projected fraction it is necessary to transform $\cos \theta_{c.m.}$ to the projected system. Using (A. 1) and (A. 4) one obtains

$$\cos \theta_{c.m.} = \frac{1 - \gamma^2 (\tan^2 \theta_X + \tan^2 \theta_Y)}{1 + \gamma^2 (\tan^2 \theta_X + \tan^2 \theta_Y)} \tag{A.9}$$

which along with (A. 6) and the result from normalization gives for the fraction

$$F(\theta_p) = \frac{\gamma^2}{\pi(A + \frac{B}{3})} \int_{-\theta_p}^{\theta_p} \int_{-\frac{\pi}{2}}^{\frac{\pi}{2}} \left\{ A + B \left[\frac{1 - \gamma^2 (\tan^2 \theta_X + \tan^2 \theta_Y)}{1 + \gamma^2 (\tan^2 \theta_X + \tan^2 \theta_Y)} \right]^2 \right\} \cdot$$

$$\frac{\sec^2 \theta_X \sec^2 \theta_Y}{[1 + \gamma^2 (\tan^2 \theta_X + \tan^2 \theta_Y)]^2} \, d\theta_X d\theta_Y \quad .$$

The first term in the integration has been done previously in section III. The second term although somewhat tedious yields a result in closed form. An extremely useful integral given by Bieriens [27] is

$$\int_0^{\frac{\pi}{2}} \frac{\sin^{2r-1}\theta \cdot \cos^{2s-1}\theta}{(p^2 \sin^2\theta + q^2 \cos^2\theta)^{r+s}} \, d\theta = \frac{\Gamma(r)\,\Gamma(s)}{\Gamma(r+s)} \frac{1}{2p^{2r}q^{2s}} \quad . \qquad \text{(A. 10)}$$

Integrating first with respect to θ_Y and then θ_X, noting in each case that the integrand is an even function of the variable of integration and using (A. 10) in doing the integral yields, after adding the first term

$$F(\theta_p) = \frac{3A + B\xi}{(3A + B)} \frac{X}{\eta}$$

where

$$\xi = \frac{3}{2} - 2\frac{X^2}{\eta^2} + \frac{3}{2}\frac{X^4}{\eta^4}$$

$$\eta = (1 + X^2)^{\frac{1}{2}}$$

$$X = \gamma \tan\theta_p \quad .$$

With some manipulation one obtains

$$\frac{F^2(\theta_p)}{1 - F^2(\theta_p)} = X^2 f_2(A, B, X) \qquad \text{(A. 11)}$$

where

$$f_2(A, B, X) = \frac{9A^2 + 6AB\xi + B^2\xi^2}{\eta^2(3A + B)^2 - X^2(9A^2 + 6AB\xi + B^2\xi^2)}$$

V. Projected Fraction - $A + B \cos^4 \theta_{c.m.}$ Case

Calculation of the projected fraction for this case proceeds along exactly the same lines for the $A + B \cos^2 \theta_{c.m.}$ case and although an order of magnitude more tedious a result of the form of (A. 11) is derived. Only the result is presented here.

$$\frac{F^2(\theta_p)}{1 - F^2(\theta_p)} = X^2 f_4(A, B, X) \qquad (A.12)$$

where

$$f_4(A, B, X) = \frac{25A^2 + 10\,AB\xi + B^2\xi^2}{\eta^2(5A + B)^2 - X^2(25A^2 + 10\,AB\,\xi + B^2\xi^2)}$$

$$\xi = \frac{15}{8} - 5\frac{X^2}{\eta^2} + \frac{39}{4}\frac{X^4}{\eta^4} - 10\frac{X^6}{\eta^6} + \frac{35}{8}\frac{X^8}{\eta^8}$$

$$\eta = (1 + X^2)^{\frac{1}{2}}$$

$$X = \gamma \tan \theta_p \quad .$$

VI. Additional Comments

Experimentally if one is observing produced secondaries for strong interactions in projected systems, for example photographing the events in 90° stereo, then by means of equations (A. 7), (A. 11) and (A. 12) one can fit the experimental data to obtain an

energy estimate and a measure of the degree of anisotropy. That is, for the isotropic case the fit is a one parameter fit for γ, while for the other cases the fit is to B and γ. Plots of $\log \frac{F^2}{1-F^2}$ vs. $\log \tan \theta$ for secondaries generated according to a C. M. distribution of the form $A + B \cos^M \theta_{c.m.}$ for $B > 0$ show two branches, corresponding to forward and backward emission with an absence of secondaries emitted at a C.M. angle of 90°. The separation of these branches depends on the magnitudes of B and M. In the theory functions the information about the branch separation is contained in $f_M(A, B, X)$ and is given by

$$\triangle = \frac{1}{2} \log\{\lim_{x \to o} f_M(A, B, X) + \lim_{x \to oo} f_M(A, B, X)\}$$

where

$$\lim_{x \to o} f_M = \frac{(M+1)A^2 + \frac{2(M+1)^2(M-1)^2 AB}{M!} + B^2\left[\frac{(M+1)(M-1)^2}{M!}\right]^2}{[(M+1)A + B]^2}$$

$$\lim_{x \to oo} f_M = \frac{[(M+1)A + B]^2}{(M+1)^2 A^2 + (M+1)(M+2)AB + (M+1)B^2} \quad .$$